8-2018

Detection of Arsenic in Skin In Vivo Using Portable X-Ray Fluorescence (PXRF) Device

Kevinraj N. Sukumar
Purdue University

DETECTION OF ARSENIC IN SKIN *IN VIVO* USING PORTABLE X-RAY FLUORESCENCE DEVICE (PXRF)

by

Kevinraj N Sukumar

A Thesis

Submitted to the Faculty of Purdue University

In Partial Fulfillment of the Requirements for the degree of

Master of Science

School of Health Sciences

West Lafayette, Indiana

August 2018

THE PURDUE UNIVERSITY GRADUATE SCHOOL
STATEMENT OF COMMITTEE APPROVAL

Dr. Linda H Nie, Chair

School of Health Sciences

Dr. Carlos Perez-Torres

School of Health Sciences

Dr. Keith M. Stantz

School of Health Sciences

Approved by:

Dr. Jason Harris

Head of the Graduate Program

To Dad, Mum, Thesrika, & Sonapareeya

ACKNOWLEDGMENTS

The completion of my research and its ultimate compilation in the form of this thesis would not have been possible if not for the support of some incredible individuals who shared my journey of graduate studies in Purdue University. Firstly, I would like to thank Dr. Linda H. Nie, my advisor whose calmness and optimism were some key features which helped me progress through this research. Her creativity and ideas always inspired me just when I thought I have exhausted all possibilities available. She supported my independent research while guiding me in the right direction. Also, she encouraged me multiple times when I struggled in my research. Not only that, she is my strong advocate for professional developments.

Next, I would like to extend my gratitude to members of my research committee. The fundamental component of this research, synthesis of arsenic-doped resin phantoms, would not have been possible without the unlimited access to Dr. Carlos Perez-Torres's lab and equipment. He helped without hesitation by demonstrating lab procedures required for making the phantoms. His energetic and enthusiastic nature always motivates me through exhausting days in lab. Besides Dr. Perez-Torres, I am grateful to Dr. Keith M. Stantz who was never out of constructive criticisms. During our meetings, he provided ideas to expand and improve my research. I also appreciate his valuable advice on professional and post-graduate career options.

Additionally, I am hugely indebted to my labmates for their tireless support and assistance. I would like to thank Xinxin Zhang for instructing and guiding me with the portable device when I started with Dr. Nie's lab during the summer of 2017. Also, I want to acknowledge her contributions during multiple attempts at making phantoms and troubleshooting

for potential errors. She was available for discussions and readily provided explanations which filled voids in my understanding pertaining to this study. In addition to Xinxin Zhang, I would like to extend my acknowledgement to Colby Neumann for his assistance with Matlab coding which helped in the data analysis portion of my research. I also had the opportunity to work with wonderful lab members who shaped a conducive and welcoming environment at lab: Michael Abel, Mindy H. Joo, Mychaela Coyne, Emma Wallens, Kyle Smith, Nicholas Farley, Sana Tabbasum, and Joseph Whitehead.

Finally, I would like to take this opportunity to thank my family members for their endless support and encouragement which helped me persist and thrive through my Masters education. Thiru Reddy was a crucial pillar of strength and held me up during my emotional stress and academic struggles these past 2 years. I would also like to thank my friends who have endured similar journeys during their graduate phases and provided me with crucial advice. Hence, the summation of all supports from the amazing people mentioned above fueled my research progress culminating into this thesis.

TABLE OF CONTENTS

LIST OF TABLES

LIST OF FIGURES

ABSTRACT

Author: Sukumar, Kevinraj, N. MS
Institution: Purdue University
Degree Received: August 2018
Title: Detection of Arsenic in Skin *In Vivo* Using Portable X-Ray Fluorescence (PXRF) Device
Major Professor: Dr. Linda H Nie

Arsenic is an element that is highly toxic in its inorganic form. It is widely distributed especially in water that becomes a primary source of exposure for human consumption. Chronic exposure can cause a variety of diseases such as lung cancer, bladder cancer, skin cancer, vascular diseases, and diabetes mellitus. Biomarkers for arsenic exposure are tissues that contain keratin such as hair, nails, and skin. Skin is an ideal biomarker due to its cumulative property that provides information about the individual long-term exposure to arsenic. Hence, a method for measuring arsenic levels *in vivo* will be useful to study the harmful effects of arsenic exposure. In this research, a portable x-ray fluorescence (XRF) device was used to determine its feasibility of detecting and quantifying arsenic in human skin. Arsenic-doped skin phantoms were used to calibrate the system. These phantoms were made using a mixture of fiberglass resin, salt solution, arsenic standard solution, and liquid hardener. In order to simulate *in vivo* measurement setting, lucite was used as a backing material that mimics the underlying soft tissue. The device was set at its maximum tube voltage of 50kV, 40μA, and silver filter. Each fluorescence data was measured for 180 seconds. The instrumental minimum detection limit (MDL) obtained using the phantoms alone is 0.17ppm. Meanwhile, the MDL obtained for a setup involving phantoms and lucite thickness of 4.44mm and 9.78mm are 0.21ppm and 0.23ppm respectively.

CHAPTER 1: INTRODUCTION

1.1 Arsenic

Arsenic is a ubiquitous element. The Earth's crust contains widely distributed arsenic among other abundantly available elements. Arsenic is a metalloid although it is generally referred to as metal; it displays both metal and non-metal characteristics ("Arsenic Public Health Statement," 2007). It is almost indistinguishable due to its inherent characteristics: colorless, odorless, and tasteless. Thus, it is difficult to detect the presence of arsenic without appropriate tests. Arsenic binds with oxygen, sulfur, and chlorine to form inorganic compounds. Meanwhile, arsenic also binds with carbon and hydrogen in its organic compounds.

1.1.1 Sources of Arsenic

Arsenic (As) is a naturally occurring element which is commonly associated with minerals and ores rather than found independently. Inorganic arsenic compounds can be found with ores with copper and lead ("Arsenic Public Health Statement," 2007). Pyrite and pyrrhotite are both iron sulfide minerals with higher arsenic concentration in the former than latter (O'Shea et al., 2015). Additionally, metal oxides display strong association with arsenic. In sediment layers and host rocks, arsenic is found with minerals such as arsenopyrite, scorodite, and iron hydroxide (Basu & Schreiber, 2013). However, arsenic is not always immobile and bound to rocks. Weathering of these minerals and ores releases arsenic into groundwater which transports this toxicity to widespread locations and ultimately human exposure. The weathering of arsenopyrite initiates oxidation to produce scorodite which undergoes incongruent dissolution to form iron hydroxides, releasing close to 96.2% of its solid arsenic into water (Basu & Schreiber, 2013). Groundwater is

not the only water medium to carry toxic arsenic levels but arsenic can contaminate surface water, drinking water, wastewater, and snow. In Poland, 97% of total arsenic concentration in snow was arsenite [As(III)], extremely toxic arsenic form, due to polluted urban air where airborne arsenic particles are most prominent (Komorowicz & BaraAkiewicz, 2016). Meanwhile, high level of arsenic is present in soils. Arsenic distribution is highly correlated with iron and sulfur abundance in soil samples (Kim, Yoo, & Baek, 2014). Hence, soils which are rich with iron and sulfur suggest the presence of high level of arsenic. In addition to natural release from arsenic-bearing minerals, arsenic is also removed from its binding by mining and smelting which further contaminate soils (Kim et al., 2014).

Besides natural processes that release arsenic from its bound state, anthropogenic activities further induce environmental toxicity. Smelting of ores containing copper and lead liberate arsenic trioxide [As_2O_3] as dust particles ("Arsenic Public Health Statement," 2007). These inorganic arsenic compound as airborne particles can get into human system via inhalation. Also, arsenic is introduced to plantations and farms via agricultural products. Rodenticides, herbicides, insecticides include arsenite due to its high solubility and immediate fatal impact (Vladimir & Florence Yan Li, 2017). Not only has agricultural arsenic product been used to control pests to promote crop growth, but it has been historically used as a tool of war strategy. Agent Blue (dimethylarsinic acid) was used as herbicides by the US troop during Vietnam War to destroy crops and reduce food supply for their enemies (Vladimir & Florence Yan Li, 2017). Agricultural uses of arsenic products contaminate food sources which endanger human health status. Not only regular dietary foods, but these agricultural materials and geological features can lead to accumulation of arsenic in tobacco products. Tobacco leaves absorb arsenic from farming

factors such as soils, pesticide, and fertilizer (Lazarević et al., 2012). This suggests that any products based on these arsenic contaminated tobacco leaves will contain residual levels of arsenic as it enters human systems.

Additionally, arsenic can be found in wood preservative, automobiles, light emitting diodes, semiconductors, volcanos, and incinerators ("Arsenic Public Health Statement," 2007). This indicates the widespread presence of arsenic, organic or inorganic, in our immediate surroundings.

1.1.2 Exposure Pathways and Metabolism in Humans

Humans can get exposed to arsenic via ingestion and inhalation. Ingestion can take place through drinking water and dietary food; there is conflicting agreement on the primary arsenic exposure between these two routes. In Vietnam, residents along the Red River Delta consume sand filtered groundwater which can result in accumulation of 1µg/g As in hair if the filtered water contains approximately 96µg/L As (Agusa et al., 2014). On the other hand, some studies suggest that food delivers higher concentration of inorganic arsenic (iAs). Based on one study, the major food sources for iAs exposure were vegetables, fruits (including extracted juices), rice, alcohol (beer and wine), and grain products (corn, wheat, and flour) (Xue, Zartarian, Wang, Liu, & Georgopoulos, 2010). Meanwhile, humans can get exposed to arsenic via breathing. As mentioned earlier, smelters and general population can be exposed to arsenic trioxide which becomes dust particles ("Arsenic Public Health Statement," 2007).

Arsenic undergoes biomethylation in the human system. Among the organs, the liver is primarily involved in methylation of iAs (Styblo et al., 1999). The iAs is converted into mono- and di-methylated species (Agusa et al., 2014; Styblo et al., 1999). Once inside the human body, iAs rapidly reaches the liver as hepatocytes express iAs content an hour after exposure and subsequently declines; mono- and di-methylated arsenic metabolites are observed within a day of exposure (Styblo et al., 1999). Arsenic is then removed out of the body via urine. Majority of the arsenic in urine is dimethyl arsenic with lesser amounts of iAs and monomethyl arsenic (Loffredo, Aposhian, Cebrian, Yamauchi, & Silbergeld, 2003).

1.1.3 Arsenic Induced Diseases

Arsenic has also been determined to be a pulmonary carcinogen. Both ingestion and inhalation of arsenic have almost similar risk potential for lung cancer development although with uncertain mechanisms (Allan, Ayse, Yan, & Craig, 2009). Inhalation provides a direct access to lungs. So, it is fair to assume that inhalation will be more carcinogenic rather than ingestion which does not introduce arsenic to the pulmonary region directly. Consumption of drinking water contaminated with increasing levels of arsenic has been shown to result in greater prevalence of lung cancer (Ferreccio et al., 2000). The iAs is special in terms of being carcinogenic to lungs via both ingestion and inhalation rather than only one of the routes (Allan et al., 2009). Lung cancer due to arsenic exposure can be exacerbated by additional risk factors. In Northern Chile, smokers had an odds ratio of 32.0 for developing lung cancer especially when combined with consumption of drinking water with an average arsenic concentration of 200µg/L (Ferreccio et al., 2000).

Besides lung cancer, ingestion of arsenic is a serious risk factor for bladder cancer among consumers. The absence rather than presence of this carcinogen is a good indicator of etiology for bladder cancer. Residents of the black foot disease endemic area (BFDEA) in southwest of Taiwan were exposed to extreme levels of arsenic in their drinking water but displayed reduced cancer incidence after clean water system was installed. In general, incidence of lung and bladder cancer dropped dramatically after highly exposed residents, especially younger generation, were supplied with clean water (Su, Lu, Tsai, & Lian, 2011). The relative risk for bladder cancer was lower for residents born post-1943, age around 30 years during installation of clean water supply, than elder residents (Su et al., 2011). High level or arsenic contamination has been proven to be associated with bladder cancer as shown by the Taiwanese population. On the other hand, low levels of arsenic have the possibilities of inducing bladder cancer risks but its etiology is not firmly established as high levels of arsenic contamination. In a study conducted in New Hampshire, majority of case subjects were active smokers with toenail arsenic accumulations range of 0.014-2.484µg/g (Karagas et al., 2004). Individuals who weren't smokers displayed almost no association between their toenail arsenic accumulation and risks of bladder cancer (Karagas et al., 2004). Hence, arsenic exposure in small amounts alone is not sufficient to present significant bladder cancer risks. In contrast to non-smokers, the risk of contracting bladder cancer was highest among smokers with greatest arsenic exposure (Karagas et al., 2004). This suggests that additional cofactor such as smoking is necessary to enhance the effect of low arsenic levels on bladder cancer.

In addition to the cancers mentioned above, arsenic has been well established as a risk factor for vascular diseases. A unique peripheral vascular disease, locally known as blackfoot disease, was

common in a specific region along the southwest coast of Taiwan (Tseng, 2002, 2005; Tseng et al., 2005). One of the visible symptoms is dark blemish forming at feet of affected individuals (Tseng, 2002) which is attributed as the origin of the local disease name. Residents with this disease display gangrene at extremities, feel numb or cold near the end of their limbs, experience cramping pain due to reduced blood flow before the onset of gangrene, and peripheral arterial pulse waves (Tseng, 2002, 2005; Tseng et al., 2005). Another indication of blackfoot disease is ulcer formation (Tseng, 2002). Most of the patients succumbed to amputation of their lower limbs (Tseng, 2002; Tseng et al., 2005). Not every exposed residents developed peripheral vascular disease. It could be due to individual variable factors such as genetics and environment; individuals capable of efficient secondary arsenic methylation have reduced risk of developing peripheral vascular disease (Tseng et al., 2005). Residents with either well water or tap water as their drinking source displayed different incidence rates; occurrence of blackfoot disease also decreased after clean water via tap system was installed (Tseng, 2002, 2005). This indicates that a link exist between arsenic exposure and development of blackfoot disease.

Diabetes mellitus is one of the determinants for peripheral vascular disease and coronary heart disease (Lai et al., 1994; Rahman, Tondel, Ahmad, & Axelson, 1998). There is strong correlation between arsenic exposure and development of diabetes mellitus. Prevalence of diabetes was highly correlated with total arsenic exposure; the greater the arsenic accumulation, the greater the diabetic prevalence (Lai et al., 1994). However, there are other factors that affect diabetes prevalence among exposed individuals such as age, gender, and lifestyle. In the arsenic hyperendemic region of Taiwan, both genders displayed higher prevalence of diabetes mellitus at

older age (Lai et al., 1994). Meanwhile, active subjects had lower prevalence of diabetes than those who were inactive (Lai et al., 1994).

1.1.4 Skin Diseases

Several studies have reported strong association between arsenic exposure and skin diseases, the visible signs of health degradation among victims. Arsenic speciation based on urine samples from subjects with skin cancer have identified greater levels of total arsenic and monomethyl arsenic but smaller level of dimethyl arsenic than they are among healthy individuals (Hsueh et al., 1997). Arsenic exposure does not cause all types of skin cancers. Among the skin lesions, squamous cell carcinoma and basal cell carcinoma are common among exposed population while malignant melanoma shows almost no association with arsenic poisoning (Guo, Yu, Hu, & Monson, 2001).

1.1.5 Biomarkers of Arsenic Exposure

The manifestation of arsenic exposure can be qualitatively determined based on observation of signs and symptoms. Abnormal visual appearances on the skin layer are an easy and immediate method to determine exposure to arsenic. Skin disorder such as keratosis is an alternative biomarker to assess subjects in identifying arsenical exposure when absolute evaluation of arsenic source is not available (Rahman et al., 1998).

Biomarkers with potential for quantitative analysis are a better option instead of relying on signs and symptoms which are subject to individual interpretation. Arsenic targets regions in human body with abundance of keratin where it binds with the sulfhydryl component in keratin (Agusa

et al., 2014). Some human tissues with keratin are nail, hair, and skin. These tissue samples provide good record on long term arsenic exposure. For example, hair is a good indicator of cumulative arsenic exposure (Agusa et al., 2014). However, hair is not an ideal biomarker for assessment using XRF analysis due to its small surface area. Nails are usually extracted from individuals and can present logistic errors. Also, it is subjected to destructive sample preparation for analysis using methods like inductively coupled plasma mass spectrometry (McIver et al., 2015). On the other hand, skin is an ideal biomarker for XRF analysis due to larger surface area. In addition to that, a particular location on the human body can be marked and repeated measurements can be performed to study long term arsenic exposure. Most importantly, arsenic exposure can manifest into skin diseases such as cancer and therefore skin is the most relevant biomarker for this study.

Besides these tissues, another common biological sample that is used to assess arsenic level in human body is urine. Urinary samples are collected to assess individual arsenic metabolic capacity (Tseng et al., 2005). While hair is used to evaluate chronic exposure, urine is good for acute exposure (Agusa et al., 2014). Also, urine is a better option to distinguish the various arsenic species as processed by the human system (Agusa et al., 2014). Some arsenic species that can be detected are dimethylarsinic acid, monomethylarsonic acid, arsenobetaine (Xue et al., 2010), inorganic arsenite, and inorganic arsenate (Tseng et al., 2005). Organic arsenic such as arsenobetaine, found in seafood, is not harmful and is usually removed in its original form (Tseng et al., 2005). On the other hand, inorganic arsenic is the element of interest due to its toxicity.

1.2 X-Ray Fluorescence (XRF)

1.2.1 Principles of XRF

X-ray fluorescence (XRF) is a physical phenomenon where a high energy x-ray or gamma ray is used to remove an orbital electron in a material which will then release a secondary or fluorescent x-ray specific to an element. This physical phenomenon is commonly applied to elemental analysis. The primary physical interaction involved here is photoelectric effect. An x-ray or gamma ray with sufficient energy is used to bombard an electron in the inner orbits of an atom. The incident photon must have energy greater than the binding energy of an electron in order to eject it from its respective shell. The released electron is referred to as photoelectron which is a result of the aforementioned photoelectric effect. The residual energy from the incident photon after overcoming binding energy is transferred into kinetic energy for the photoelectron to travel beyond the atom. Now, another electron from a higher orbit will drop down to fill up the vacant spot left by the photoelectron. This transfer of electron releases energy in order to conserve energy, equivalent to the difference between the binding energies of initial and final positions of the migrating electron, in the form of a photon. The emitted photon known as fluorescence x-ray with characteristic energy is unique to the element present in the sample. Another possible emission due to conservation of energy is the Auger electron. If the excess energy is not released via fluorescence x-ray, then this surplus energy will be used to knock out an electron from higher orbital shells. Atoms have multiple orbital shells identified as K, L, M, N and so on. Each element has a specific energy configuration or order between its shells. The characteristic energy and fluorescence x-ray intensity can be used to determine the amount of available element in the sample.

1.2.2 Portable XRF

Portable or handheld XRF device is used in a wide range of fields and applications that require elemental analysis. This includes geological sampling in mining activities and elemental identification in recycled metals. The portable XRF device used in this research is the Niton XL3t GOLDD+ XRF Analyzer by Thermo Fisher. It features a silver (Ag) anode tube with voltage and current ranges of 6-50kV and 0-200µA respectively. Also, various combination of filter material is available. This device collects information about the fluorescence using a silicon drift detector (SDD). Instead of standard SDD, the geometrically optimized large area drift detector (GOLDD) has greater surface area for better detection. This thermoelectrically cooled detector has 25mm^2 of surface area and 1mm of thickness.

The XRF device is powered by lithium-ion battery which is rechargeable. Also, a charge-coupled device camera is in place to locate and position the sample in the beam's eye-view. Its settings can be adjusted via the tiltable touch screen display which also produces results of test with peaks and list of elements. For the purpose of this research, the data was transferred to a computer via USB and accompanying software. A test stand is provided with the device to hold the analyzer in place for the test duration in lab. The test stand provides shielding from external sources of radiation and prevents any radiation leakage. There are safety interlocks that prevent use of the device if not properly positioned in the test stand. The device can be used beyond the test stand but requires an extra component fixed to the tube output to override the interlocks. A trigger is applied to turn on the x-ray tube which will then feature flashing lights on its sides for safety, indicating that the device is emitting x-ray beam.

In addition to its electronic specifications, the device weighs about 3lbs with small dimensions. Its lightweight and small size makes it portable and mobile. Not only that, it produces efficient detection of elements within short duration of sampling time. This makes it ideal to be transported to places where desired testing takes place. Patients with metal contamination do not need to come to lab. Instead, the XRF device can be brought to them. Also, the cost of transportation and sample processing is greatly reduced making it suitable for clinical studies in remote areas.

This technology can analyze samples non-destructively, without causing any damage to the material of interest. The samples for this method of analysis can be solid, powder, or even liquid. Hence, sample preparation is also easy and does not involve elaborate process.

1.2.3 XRF for the *In Vivo* Quantification of Metals

XRF technology has been used extensively to quantify metals in human body based on *in vivo* measurements. The primary motive for using this technology is its non-invasive ability. In one study, portable XRF capability to quantify bone lead was compared against conventional KXRF equipment (Nie et al., 2011). Researchers wanted to determine if portable XRF can be developed and used for detection and quantification of bone lead non-invasively which was later affirmed (Nie et al., 2011). Another research group also investigated the application of XRF for measuring bone lead. Using synchrotron radiation and portable XRF device, the contrasting and overlapping features in data output were determined (Groskopf, Bennett, Gherase, & Fleming, 2017). Besides establishing the effectiveness of using portable LXRF for bone lead quantification, further efforts were made to identify the optimal settings combination that will reduce the minimum detection

limit (MDL) (Aaron James Specht, Weisskopf, & Nie, 2014). The MDL achieved by this research group for bone lead quantification is 2.9 µg/g (ppm) with 2mm of soft tissue based on 180 seconds measurement time (Aaron James Specht et al., 2014).

Besides lead, another metal studied using XRF principle is cadmium. Three XRF systems, all consisting of cadmium-109 (either 0.35GBq or 2.8GBq) excitation source but different detectors (two of which are HpGe and one is lithium drifted silicon [Si(Li)]), were compared to determine their ability to quantify bone cadmium based on MDL (Popovic, Chettle, McNeill, & Pejović-Milić, 2006). Best detection system was cloverleaf design which consisted of four HpGe that resulted in MDL of 2.1 µg/g (ppm) with 3mm of wax covering the phantoms to simulate soft tissue (Popovic et al., 2006).

Additionally, portable XRF device was studied to determine and demonstrate its validity to quantify bone strontium based on children population (Aaron J. Specht, Mostafaei, Lin, Xu, & Nie, 2017). It has also been used to measure toenail manganese and mercury *in vivo*. The MDL achieved for manganese and mercury are 3.65 µg/g (ppm) and 0.55 µg/g (ppm) respectively using 1mm thick nail phantoms placed on 1cm thick lucite which mimics soft tissue based on 180 seconds measurement time (Zhang, Specht, Weisskopf, Weuve, & Nie, 2018).

1.2.4 XRF for the *In Vivo* Quantification of Arsenic in Skin

The XRF technology has also been used to investigate the detection and quantification of arsenic in human skin. One of the earliest work done in this field employed a system with iodine-125 as its fluorescing source and achieved a range of MDL from 2.6±0.5 µg/g (ppm) to 5.7±1.1 µg/g

(ppm) (Studinski, McNeill, Chettle, & O'Meara, 2005). The same research group used a 50 W x-ray tube with molybdenum target with 35kV and 200µm molybdenum filter to achieve a MDL of 0.40±0.06 µg/g (ppm) (Studinski, McNeill, O'Meara, & Chettle, 2006). In this research, various setting combinations were explored and its MDL measured. Based on these two studies alone, it is evident that the use of x-ray tube technology instead of radioactive source contributes to great improvement in arsenic detection limits.

Later, human samples were used to validate the effectiveness of portable XRF system in measuring arsenic. Clippings of human finger and toe nails were extracted from subjects for analysis (McIver et al., 2015). This study tested portable XRF device on extracted nail clippings from a population affected by arsenic contamination, compared the results against that obtained by ICP-MS, and determined the valid data range to identify suitable settings for portable device (McIver et al., 2015). XRF and ICP-MS results conformed to each other better when the mass of nail samples were greater, 20-30mg (McIver et al., 2015).

Portable XRF (4W Au anode Olympus InnovX Delta) and benchtop XRF (25W Ag anode by XOS) systems were compared in measuring selenium and arsenic (Shehab, 2016). The MDL for portable XRF is 0.59±0.03 µg/g (ppm) for arsenic based on 1 minute measurement time while the MDL for the benchtop system produced 0.35±0.01 µg/g (ppm) based on 30 minutes measurement time (Shehab, 2016). Similarly, two portable XRF devices, Olympus InnovX Delta and InnovX Alpha, were tested against each other to measure arsenic (Desouza et al., 2017). Both devices employed 40kVp but different tube current for each system; 37µA or 17µA for the former and 20µA for the latter (Desouza et al., 2017). Based on 120 seconds of measurement

time, the better MDL of 0.462±0.002 µg/g (ppm) was achieved by the Delta model (Desouza et al., 2017).

1.3 Objectives of the Project

The aim of this research is to determine the feasibility of using portable XRF device for detecting and measuring arsenic in human skin. As mentioned earlier, there are a few biomarkers for arsenic such as hair, nails, and skin due to their keratin levels. In this study, skin will be the biomarker of choice. Skin, especially under the feet close to heels, is one of the thickest site and furthest from bone. The distance of bone from skin surface is an important consideration here to avoid a possible interference from Pb Lα if the individual is exposed to both arsenic and lead contamination. Not only that, the surface of skin is exposed and a specific area can be marked for repeated or multiple readings. The same site can be used to study cumulative arsenic exposure over a period of time. Also, there is insufficient data of arsenic accumulation in human skin available. Hence, skin under the heels is an ideal *in vivo* measurement site.

The first step in this research is to perform system calibration using arsenic-doped skin phantoms. In order to do this calibration, skin phantoms that simulate the photon interaction properties of human skin will be produced. The composition of skin phantoms and steps for making phantoms are determined. Then, the effect of underlying soft tissue will be studied to understand its contribution towards arsenic signal intensity from superficial layers of skin.

Finally, the minimum detection limits for the system will be determined. These values will be compared with other similar studies that have measured arsenic with portable XRF systems. Any

differences in values will be discussed with plausible explanations. The long term goal is to develop this portable XRF device to record arsenic exposure in human population based on skin under the heels as measurement site.

CHAPTER 2: MATERIALS AND METHODS

2.1 Portable XRF Skin Arsenic Measurement System

In this research, a customized portable XRF device was employed (Niton XL3t GOLDD+, Thermo Fisher Scientific Inc., Billerica, MA). This device, shown in Figure 1, is compact with optimized geometry. Throughout this research, this portable XRF device was used to collect all fluorescence data.

Figure 1 XL3t GOLDD+ portable XRF device from Thermo Fisher Scientific

The device was fixed to a stand, provided by the manufacturer, with shielding lid as shown in Figure 2.

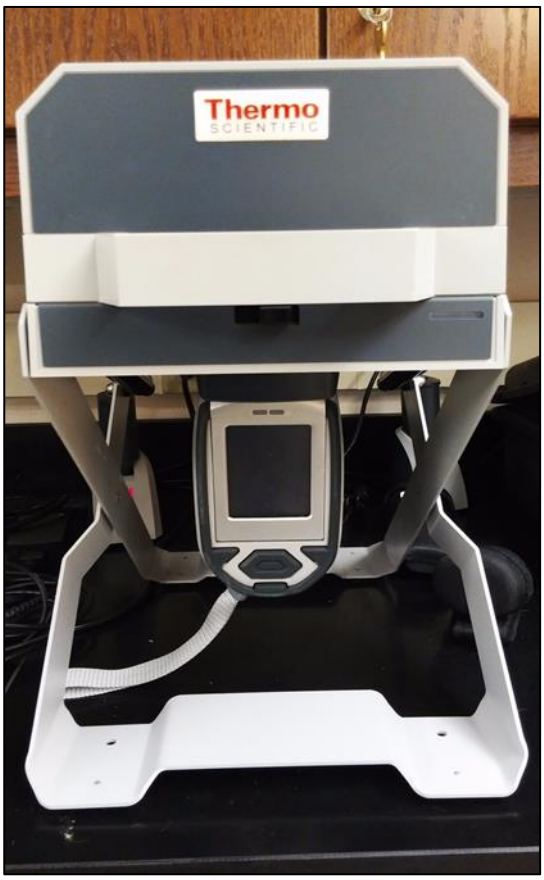

Figure 2 Device was fixed to the base of stand with shielding lid

This shielding lid prevents any radiation leakage and contamination from external radiation sources. Since the device is attached to the stand, the setup is simply referred to as stand mode. An alternative way to using this device to take measurement is to simply hold it in a point-and-shoot fashion directed towards the sample. This method is useful for *in vivo* measurements where the geometry and angle is subject to variations. However, the device has to be stationary with constant geometry for the purpose of data collection in this research. Hence, the device is affixed to the bottom of the stand to direct the beam in an upward manner. The cross sectional area of beam spot in contact with the phantom surface is approximately 1.13cm^2 with a diameter of

1.2cm. An interlock is present between the device and stand. It is a safety feature that enables the user to handle the device safely and prevents any mishandling that could lead to unnecessary radiation exposure. A highlight of this customized device is that it allows user to specify settings such as tube voltage, current, and filter. Its maximum power is 50kV. In this study, the settings were chosen to be 50kV and 40μA. Silver filter combination was used. Once the type of sample is chosen, the camera is activated and aids to position the phantom so that it aligns with the x-ray beam. X-ray beam is generated when the trigger is pressed; flashing lights on the sides turn on instantaneously as an indication of x-ray beam production and for additional safety precautions.

2.2 Arsenic-doped Skin Phantoms and System Calibration

The system calibration required phantoms that replicate human skin in terms of photon interaction properties. Total photon attenuation at 10.54 keV (As Kα) and photoelectric absorption at 22.1 keV (Ag anode) was used as the basis for synthesizing skin phantoms. These information for fiberglass resin, salt, human skin, and phantoms were obtained from XCOM website and presented in Table 1 below. Using the obtained values, a fiberglass resin and salt mixture was determined to produce skin phantoms. Since the resin matrix was fixed from the manufacturer, the photon interaction properties based on its elemental composition cannot be changed. In order to alter the photon interaction properties of resin, table salt was proposed as an additional ingredient. This method has been used in another study to produce toenail phantoms (Zhang et al., 2018). Based on the information in Table 1, the proportion of 97% resin and 3% salt was calculated to best represent human skin. The difference in values between skin phantom and human skin is due to the photon attenuation and photoelectric absorption contribution from

additional elements present in human skin in trace amounts which were not included in the calculation here.

Table 1 Elemental composition and density of resin and salt to produce skin phantoms that mimic human skin based on total photon attenuation and photoelectric absorption properties

Substance	Major elements (%)	Density (g/cm^3)	Total attenuation at 10.54keV As K-alpha (cm^2/g)	Photoelectric absorption at 22.16keV (cm^2/g)
Resin	C (60), O (35), H (5)	1.20	3.03	0.25
Salt	Na (39), Cl (61)	2.17	35.26	3.77
Skin phantom	C (58.2), O (33.95), H (4.85), Na (1.17), Cl (1.83)	1.23	3.99	0.35
Human skin	O (62), C (23), H (10), N (5)	1.10	3.83	0.32

A total of four attempts were made to produce skin-equivalent phantoms. The general steps involved in this process will be presented first before describing the specific changes made in later trials to improve the quality of phantoms.

Silicone molds were first prepared by rinsing them in deionized water to remove any impurities. Once the molds were dry, they were labeled with permanent marker to distinguish their respective arsenic concentrations. Then, empty 50ml polypropylene beakers were placed on the

mass balance to record individual masses. Approximately 20ml of fiberglass resin (Bondo Corp., Atlanta, GA) was poured into each container. Once again, the containers with resin were measured to determine the actual mass of resin. Based on the recorded resin masses, the mass of salt that is required for each concentration was calculated using the proportion of 97% resin and 3% salt.

The calculated salt (Morton Salt Inc., Chicago, IL) mass was added to a small plastic plate for each concentration. Whole salt cannot be added to resin directly because it will not dissolve. Hence, deionized water in small volume was added incrementally to the plastic plate until salt was completely dissolved. This salt solution was then added to resin. Since arsenic distribution in human skin is unknown, it was assumed to be homogeneous for the purpose of making phantoms. Thus, the mixture was placed on a hot plate and a magnetic stir bar added to help produce homogeneous solution. Using the total mass of the resin and salt mixture, the amount of arsenic for each concentration is determined in terms of mass. Mass was then converted into volume which was drawn from arsenic atomic absorption standard solution with 999±4 mg/L concentration (Sigma-Aldrich Corp., St.Louis, MO). Pipette (Biotix Inc, San Diego, CA) was used to transfer arsenic volume into each beaker. After arsenic was transferred, drops of liquid hardener were added and the mixture was allowed to continue stir well. So, phantom mixture contained fiberglass resin, salt solution, arsenic solution, and liquid hardener. Finally, the homogeneous mixture was poured into the labeled molds. All molds were left under a fume hood for close to two weeks to harden and remove the strong odor from resin.

The phantoms had arsenic concentrations of 0, 5, 10, 15, 20, and 25 ppm. Once the phantoms have hardened, they were removed from their silicone molds and sealed in small and transparent plastic bags. These little bags were vacuumed prior to sealing in order to prevent any formation of air bubbles that could cause attenuation and introduce errors to the measured data signal. The bags were once again labelled according to the arsenic concentrations in each phantom for easy identification. Phantom thickness was measured using a micrometer screw gauge which yielded measurements in inches. These data was then converted to millimeters for better comparison with available phantom and skin thickness data.

During Trial 1, only 5-8 drops of liquid hardener were added to the phantom mixture. These phantoms were then left under a fume hood for almost three weeks to harden. In the second trial, silicone molds with round horizontal cross section and trapezoidal vertical cross section were used due to availability in lab. Since these molds were taller than the phantom thickness required for this study, the desired thickness was achieved by first calculating the volume of mold for a height of 1mm and 2mm. Then, the mass of phantom solution was determined based on the volume of mold and density of phantom mixture. Also, liquid hardener was increased to 10-15 drops. Round and cylindrical silicone molds with approximately 2mm of thickness were used in Trial 3 instead of previously mentioned mold shape. Not only that, a dilute concentration of arsenic solution was made using 999±4 mg/L arsenic atomic absorption standard solution. 10ml of the standard solution was added to 40ml of deionized water to produce a 200ppm solution. The arsenic standard solution was diluted to prevent excessive errors due to using pipette with capacity in the microliter range. Also, five different spots on each phantom were measured to assess arsenic homogeneity.

In the final Trial 4, 12-15 drops of liquid hardener were added to phantom solution. This process lasted approximately 40 minutes for each arsenic concentration with each new ingredient such as salt solution, arsenic solution, and liquid hardener droplets added at 10 minutes intervals. For each arsenic concentration, there were two phantoms, an extra to serve as backup. A total of three spots on a single phantom were marked as X, Y, and Z. Each of the spots was measured for 180 seconds using a stopwatch since the device does not have an installed timer which can stop the measurement at the 3 minutes mark. Hence, each phantom took approximately 9-12 minutes including time to switch between different spots.

The effects of soft tissue underlying human skin were studied using lucite. Three different lucite thickness of 0.51, 1.56, and 2.22mm were available for this study. These lucite slabs were stacked on each other to get a range of thickness from 0.51mm to 13.90mm. In order to determine if underlying soft tissue interferes with arsenic signal intensity, fluorescence measurements were done by having the arsenic phantoms located in between x-ray beam and lucite slabs. Two different measurements were performed using lucite. Firstly, a 25ppm arsenic-doped skin phantom was measured with the range of lucite thickness mentioned above. Next, all phantoms were measured using two different lucite thickness of 4.44mm and 9.78mm.

2.3 Data Analysis

The fluorescence data was transferred via USB cable to a desktop computer in lab. Using software provided by the manufacturer, the data was downloaded and exported in the form of Excel spreadsheet. This spreadsheet was then subjected for analysis using Matlab. For spectral

analysis, single-peak fitting was conducted. The As Kα peak was fitted with energy range of 10.2-11.03keV. Arsenic peak was fitted using Equation 1 and non-linear least squares algorithm. The background was described as exponential.

$$f(x) = Ae^{[-0.5\left(\frac{x-B}{C}\right)^2]} + Fe^{xG} \qquad (1)$$

In this equation, A refers to the amplitude of As Kα peak. B represents the peak position while C is the standard deviation. F is the amplitude of background counts. X is the channel number.

The highest concentration phantom, 25ppm was fitted first to identify the position and width of the As Kα intensity peak. Width can be determined from the value of c in the equation above. 25ppm phantom was chosen as it yielded the highest signal intensity for the available range of arsenic-doped skin phantoms. Then, this fit was applied to measure the net count rates of the phantoms with lower arsenic concentrations.

CHAPTER 3: RESULTS

3.1 Spectrum of Phantom Measurements

As mentioned before, a total of four trials were made to produce valid skin phantoms by the end of this research. Each consecutive phantom making process involved corrections to errors made from the previous attempts. The results from all four sets of phantoms, except for the first attempt, will be presented here because phantoms from Trial 1 did not harden regardless of extensive time allowed and had to be eliminated.

In order to study the effects of skin thickness on arsenic signal intensity, two sets of round phantoms were produced during the second trial. The phantom surface area was approximately 7.07cm^2 with a diameter of 3cm. A sample phantom from this trial is shown in Figure 3.

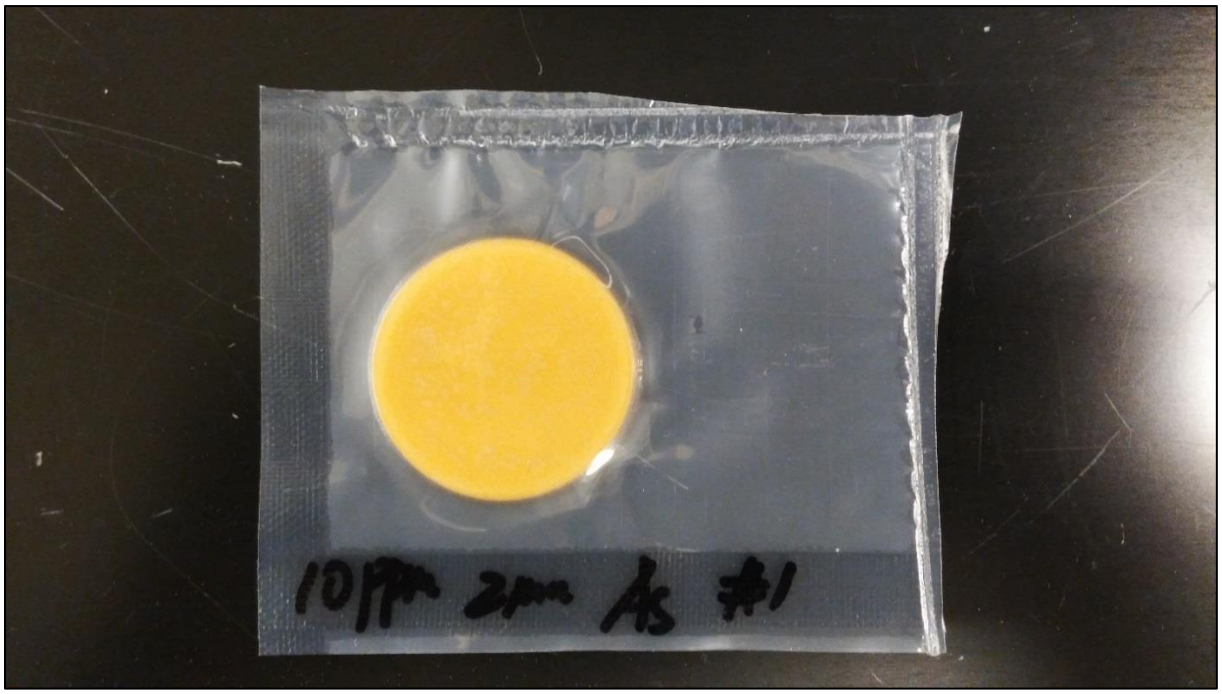

Figure 3 10ppm arsenic-doped skin phantom from Trial 2

Initially, the phantoms were intended to be at 1mm and 2mm of thickness but the final measurements were different. Thus, these phantoms were categorized generally as either thin or thick based on measured thickness for each given arsenic-doped skin phantom. The recorded thickness for all the phantoms from this Trial 2 is presented in the table below. Since the x-ray beam was aligned to the center of phantoms and fluorescence data recorded, the thickness was measured for only one position and taken as phantom thickness as the surface was even and uniform except for the edges. The fluorescence data for this set of phantoms are presented in the following section for calibration lines.

Table 2 Measured thickness for arsenic-doped skin phantoms from Trial 2

Category	Arsenic (ppm)	Measured thickness (mm)
Thin	0	1.18
	5	1.35
	10	1.68
	15	1.00
	20	0.91
	25	0.85
Thick	0	1.73
	5	2.06
	10	2.11
	15	1.79
	20	1.47
	25	1.91

During the third trial, a different silicone mold from the previous trials was used. The molds were round but with greater surface area resulting in phantoms with approximately 18.1cm^2 with diameter of 4.8cm. A sample phantom from this trial is shown below.

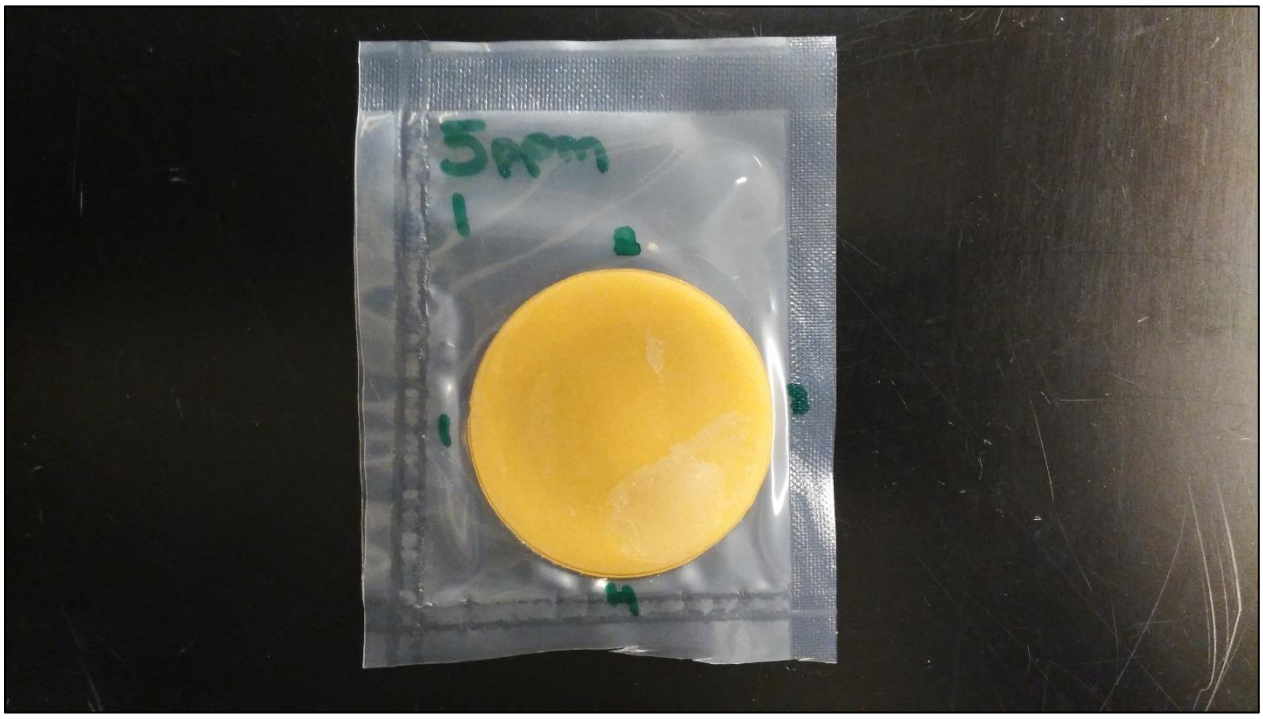

Figure 4 5ppm arsenic-doped skin phantom from Trial 3 with numbered labels for measurement sites

For each arsenic concentration, there were two phantoms to serve as backup except for 0ppm and 25ppm. The second phantom for 25ppm was shifted before it hardened causing smearing and uneven surface. Since the molds had same thickness, all phantoms were approximately similar and thickness was not measured for this set of phantoms. Meanwhile, there was visible change in phantom opacity from initial time when phantoms were made and final removal from their respective molds. Fluorescence data was collected from five different spots, center and four spots at right angles to each other as seen in Figure 4, for each phantom. This was done to determine if

the arsenic distribution in the phantoms was homogenous. Again, this data was used to plot calibration lines and is presented later.

Phantoms produced from Trial 4 used the same silicone molds as in Trial 3. Hence, the phantoms have similar surface area and diameter. Some phantoms made during this attempt are shown in Figure 5. Once again, there were some spots on phantoms where the opacity was not uniform.

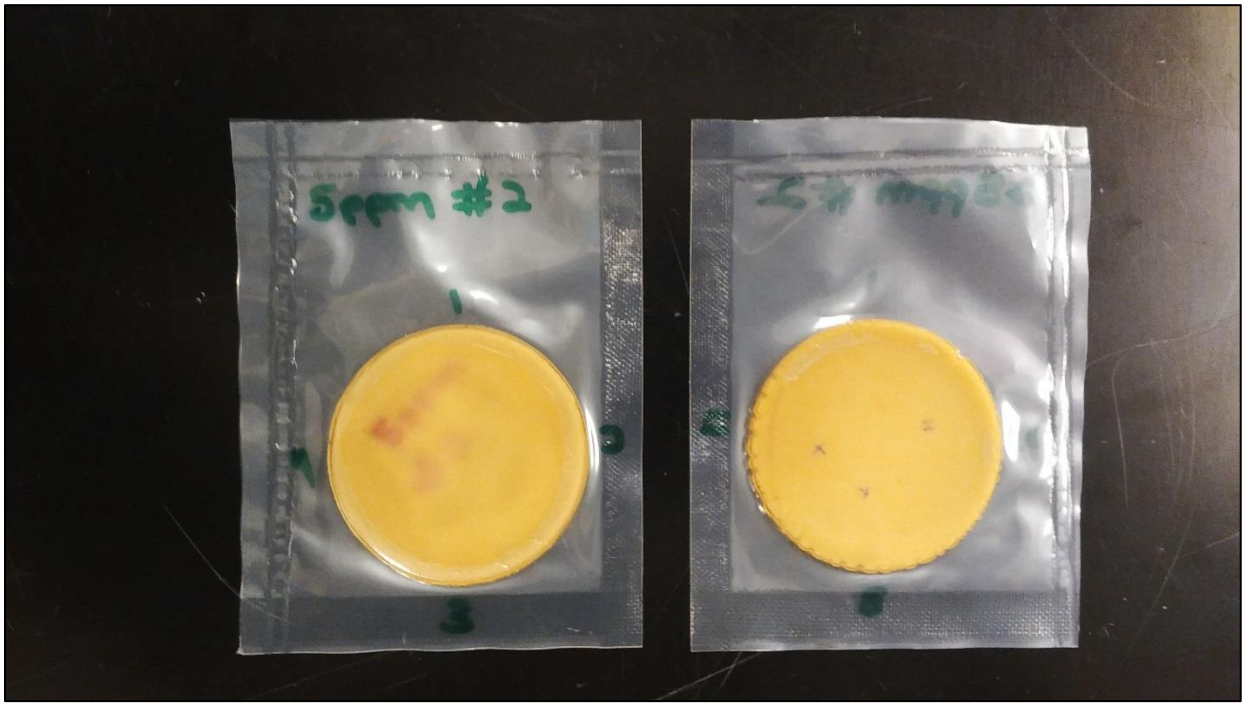

Figure 5 Phantoms produced from Trial 4. The phantom on the right shows the three spots marked as X, Y and Z for measurement of fluorescence and thickness data

The full energy spectrum from the arsenic-doped skin phantoms has a range of 0-60keV although available data is up to 50keV.

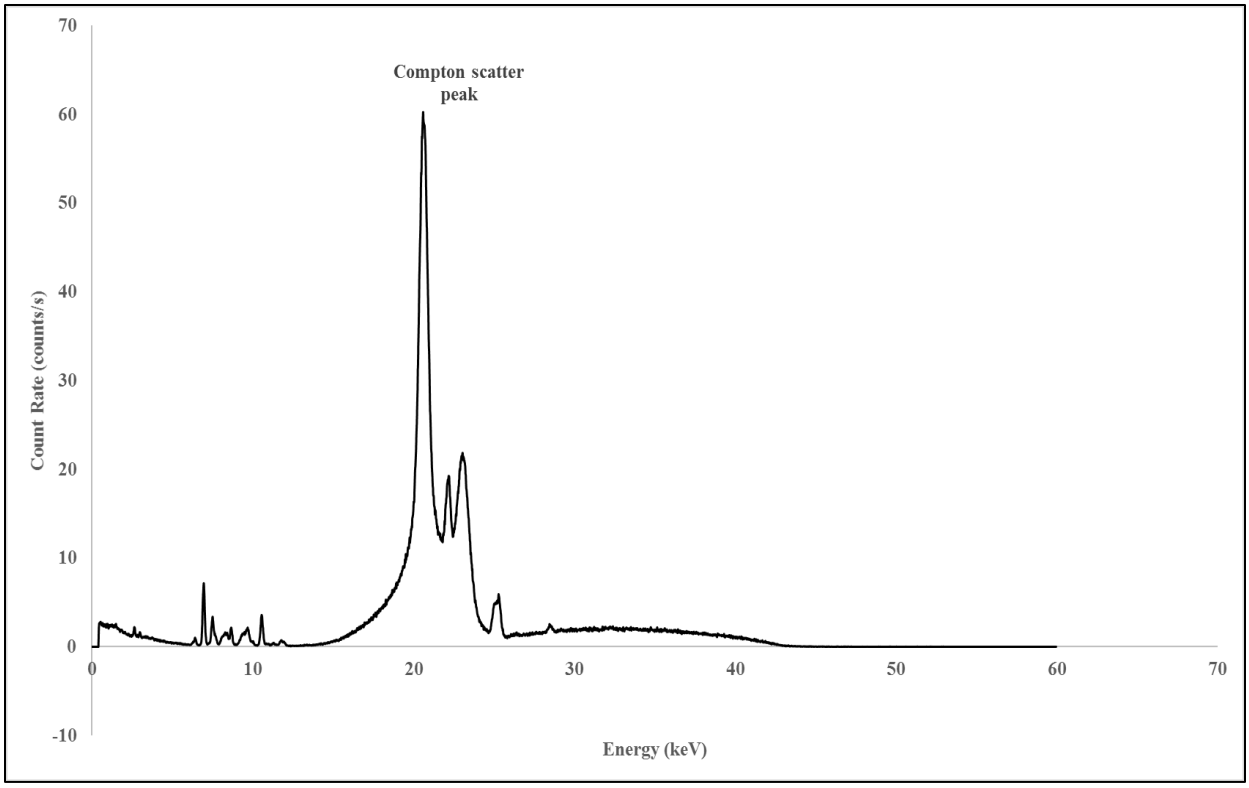

Figure 6 Full energy spectrum from 25ppm arsenic-doped skin phantom

In the full energy spectrum shown in Figure 6, the highest intensity peak is observed at around 20.5keV. This Compton scattering peak originates from the silver (Ag) anode tube as it undergoes scattering after interaction with the phantoms. There are multiple characteristic energy peaks visible in the lower energy spectrum especially close to the As Kα peak as shown in Figure 7. Between the 5keV and 13keV energy range, some elemental characteristic x-ray peaks such as 6.41keV (Fe Kα), 6.95keV (Co Kα), 7.50keV (Ni Kα), 8.66keV (Zn Kα), and 9.68keV (W Lβ1) are present. Since these peaks were observed for both 0ppm and 25ppm phantoms, they mainly originate from the device components. For example, the device is shielded with iron material which contributes the Fe Kα peak at 6.41keV. The arsenic peaks, Kα and Kβ, are also present in

the spectrum. The As Kα is significantly observed at 10.54keV while the As Kβ produces relatively lower signal even in the 25ppm phantom.

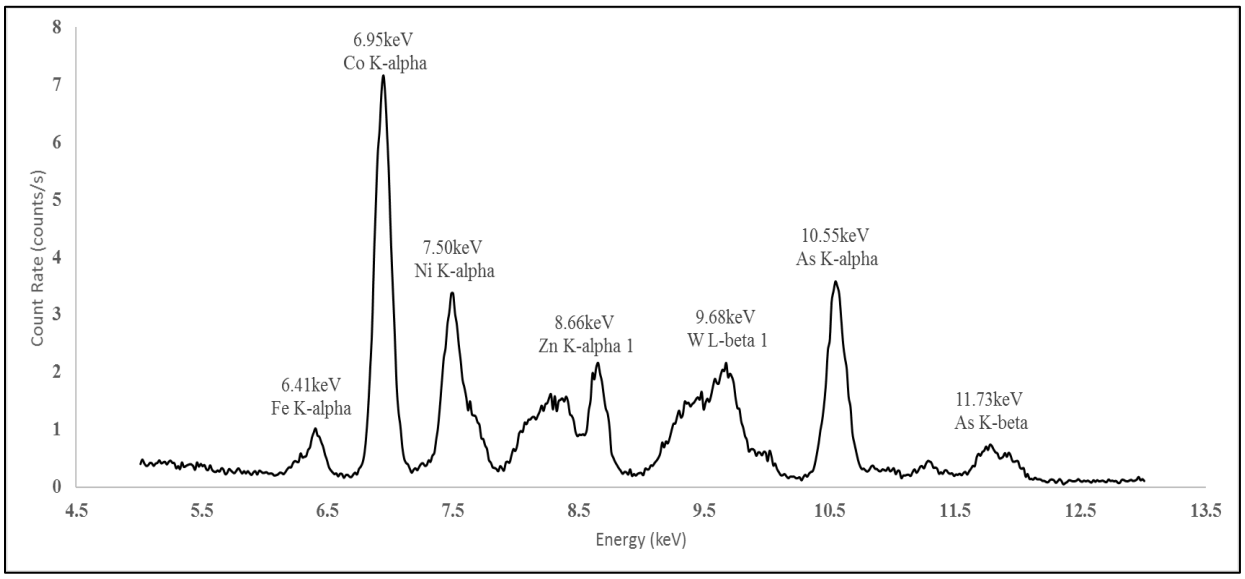

Figure 7 Low energy spectrum displaying multiple characteristic x-ray peaks close to arsenic peaks based on 25ppm arsenic-doped skin phantom

3.2 Spectral Analysis

The element of interest in this study is arsenic whose characteristic x-ray peaks occur at 10.54keV (As Kα) and 11.73keV (As Kβ). Since the As Kβ produced weak signal intensity even for the highest available arsenic-doped skin phantom, only data for As Kα was fitted for spectral analysis. Figure 8 shows the As Kα peak fitted for the 25ppm phantom which was measured for 180 seconds.

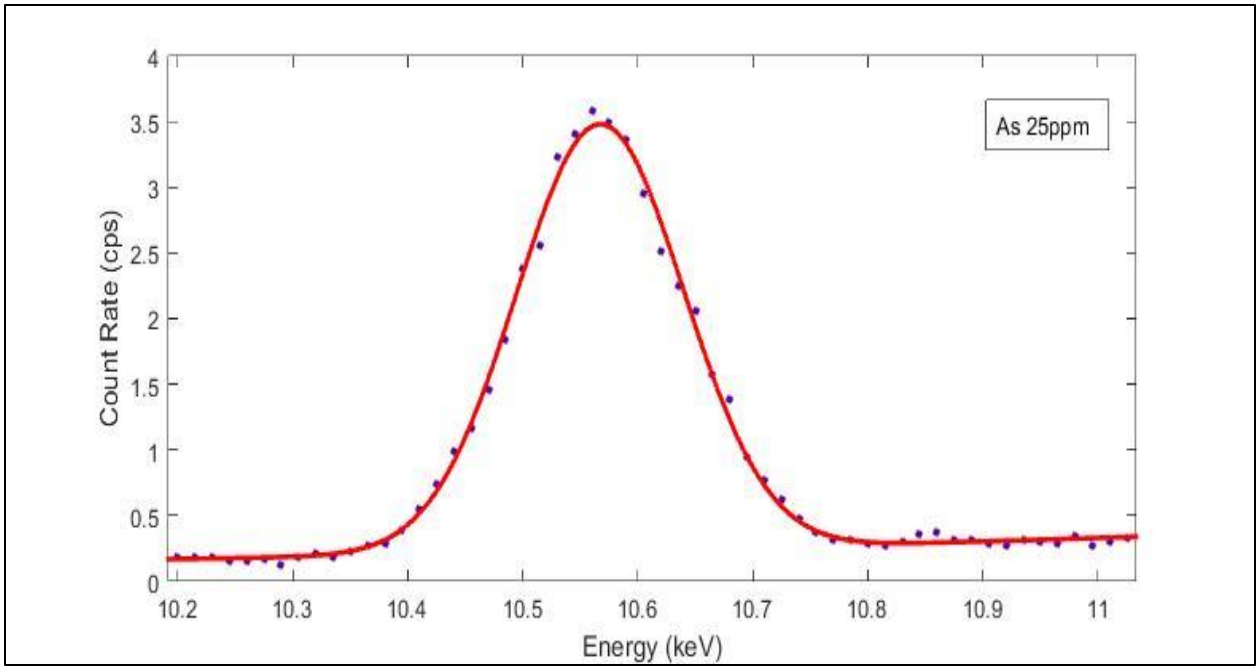

Figure 8 Arsenic Kα peak for 25ppm phantom fitted with Gaussian equation

The As Kα peak follows a Gaussian distribution. Commonly, Pb Lα will contribute to the energy peak close to As Kα if it is present in the system. Pb Lα has energy of 10.55keV which has high potential of interfering with As Kα at 10.54keV. Since phantoms with arsenic concentrations have As peaks for certain, then it is difficult to distinguish the origin of the peak. Thus, the 0ppm phantom was used to determine the presence of lead in the measurement system. Since the 0ppm spectra did not exhibit any peaks in that energy region, then it was ascertained that Pb is not present in this system. Hence, there is no contamination from Pb that overlaps and interferes with the As Kα peak intensity.

Each phantom data was analyzed using Matlab code to determine the net count rate. The count rates and other information about the phantoms from Trial 4 are presented in the following Table 3. For each phantom, there are three count rates corresponding to the three spots identified on the

phantom surface. The range of phantom thickness is between 1.31mm and 2.45mm. For 0ppm phantom, the spot thicknesses have visible deviation from the other phantoms. However, since this is just for 0ppm phantom which does not contain arsenic, the thickness is considered to be negligible. Based on the fitted curve, the reduced χ^2 values for all phantoms are in the range of 0.60 to 1.46 with an average of 0.98±0.10, indicating good fitting of the measured fluorescence data.

Table 3 Count rates for arsenic-doped skin phantoms from Trial 4 corresponding to their positions and thickness

Arsenic (ppm)	Position	Net Count Rates (cps)	X^2 Reduced	Thickness (in)	Thickness (mm)
0	X	-0.55±0.18	1.46	0.097	2.45
0	Y	-0.63±0.14	0.83	0.097	2.45
0	Z	-0.54±0.22	1.45	0.076	1.92
5	X	6.32±0.20	0.82	0.052	1.31
5	Y	7.50±0.25	1.40	0.052	1.31
5	Z	7.42±0.24	1.44	0.072	1.82
10	X	13.77±0.27	1.13	0.069	1.75
10	Y	15.24±0.28	1.13	0.069	1.75
10	Z	15.38±0.28	1.01	0.070	1.77
15	X	21.75±0.21	0.70	0.066	1.68
15	Y	23.35±0.23	0.60	0.068	1.73
15	Z	21.85±0.23	0.62	0.068	1.72

Table 3 Continued

20	X	31.62±0.28	0.72	0.073	1.84
20	Y	33.24±0.26	0.81	0.053	1.33
20	Z	29.93±0.33	1.00	0.073	1.84
25	X	39.77±0.27	0.77	0.073	1.85
25	Y	39.77±0.34	0.92	0.052	1.321
25	Z	39.52±0.38	0.77	0.074	1.880

3.3 Calibration Lines for Bare Skin Phantoms

The calibration of portable XRF device used in this study is obtained by measuring the net counts produced by the calibration phantoms during the measurement period. As mentioned in the data analysis section, the fluorescence data was fitted with an energy range of 10.2-11.03keV to include only the As Kα peak. The net count rates represented as the ±2σ area from the central position under the peak of interest was provided by Matlab. These values were multiplied with 180 seconds to obtain the net counts. Then, the calculated net counts were plotted against the arsenic phantom concentrations. Based on the information above, the calibration lines generated for the multiple sets of arsenic-doped skin phantoms using portable XRF device is presented in in this section. In the following plots of calibration line, only skin phantoms were used without any backing material. The vertical axis (y-axis) represents the net counts obtained over the measurement period while horizontal axis (x-axis) refers to arsenic concentrations using the units of ppm which is just arsenic (µg) per dry weight of resin (g).

The fluorescence data from Trial 2 which was recorded for 180 seconds is plotted and its calibration lines presented in Figure 9. Since the data is for sets of thin and thick phantoms, there are two calibration lines for comparison. Error bars are not included due to their small range which becomes invisible in the plot. The R^2 for the thin and thick set of phantoms are 0.9707 and 0.9826 respectively. On the other hand, the slope which indicates the ratio of net counts to arsenic concentration is higher for the thick phantoms compared to the thin phantoms. This is an expected result. However, the intercept for the thick phantoms was lower than that for the thin phantoms. If the phantom thickness was uniform for all arsenic concentration, then the calibration line would be shifted a little higher and the intercept for the thick phantom set will be improved.

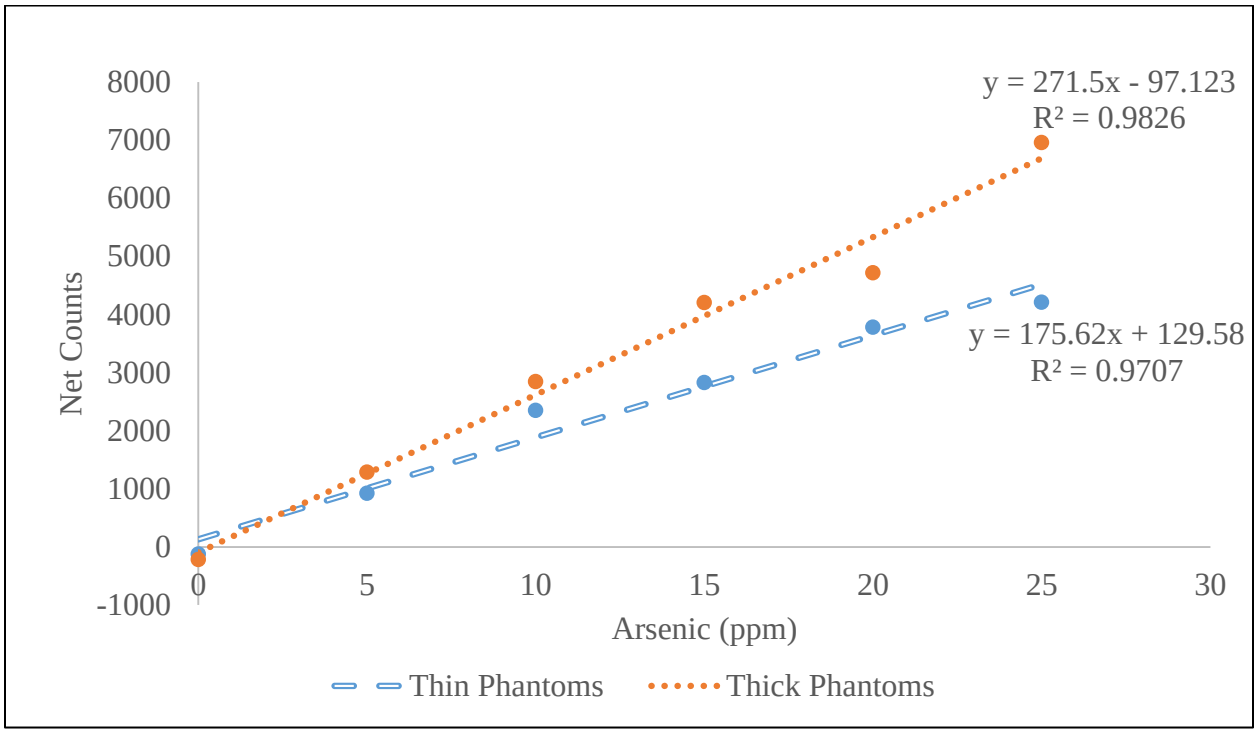

Figure 9 Calibration lines for thin and thick phantoms from Trial 2

Fluorescence data based on phantoms from Trial 3 were used to plot calibration lines. Since five spots on a single phantom were measured for arsenic fluorescence signal, there are five data points for each arsenic concentration. The multiple spot measurements were performed to assess the homogeneity of the phantoms. Also, there were two sets of data since each arsenic-doped phantom had an extra phantom for backup. The calibration lines from these two sets of phantoms are presented in Figure 10 and Figure 11 below.

The phantoms from Set 1 were evidently not homogeneous as can be seen in the widespread distribution of fluorescence data points for 10, 15, 20, 25 ppm. Data points for 15 and 20 ppm had significant deviation from the calibration line. This strongly suggested that arsenic was not uniformly distributed in the phantoms. Hence, the resulting calibration line was poor based on obtained $R^2 = 0.9453$.

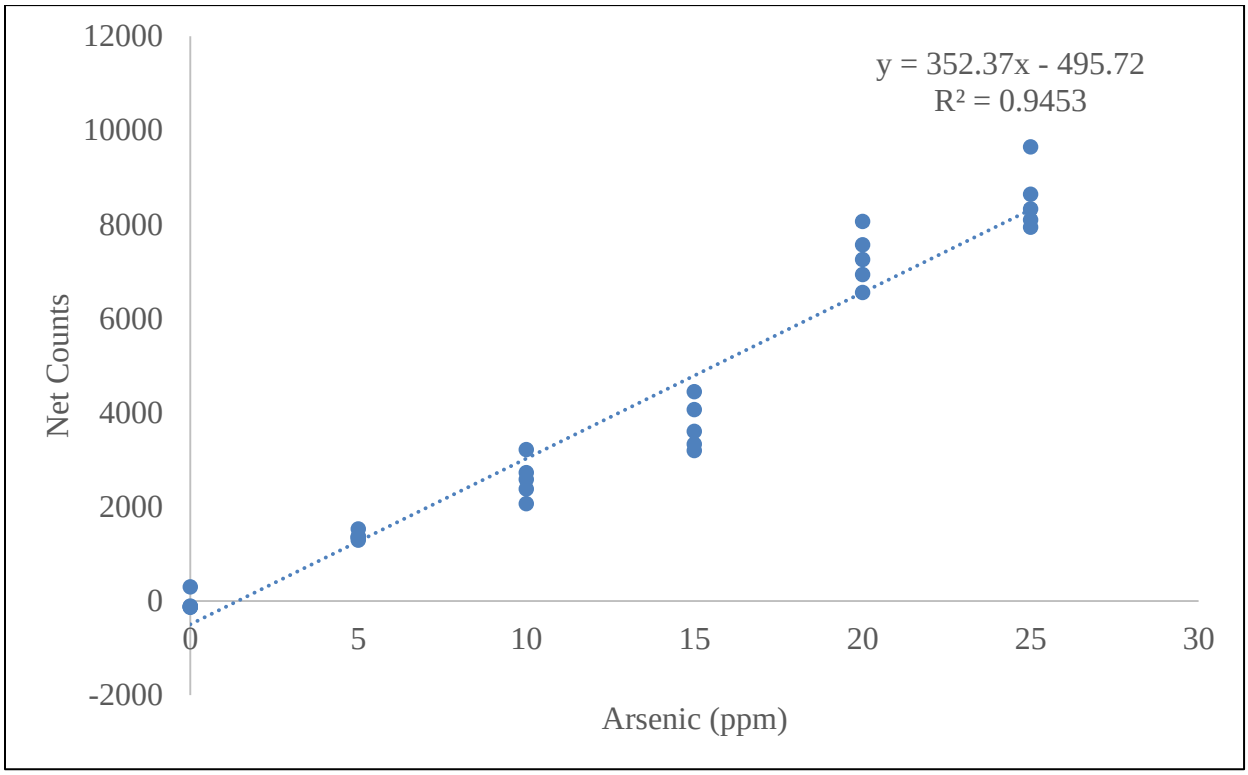

Figure 10 Calibration line using phantoms from Trial 3 for Set 1

The phantoms from Set 2 were better than Set 1. The fluorescence data points are distributed closer to each other especially for 10, 15, and 20 ppm as compared to the phantoms with same concentration in Set 1. Thus, the calibration line was improved based on obtained $R^2 = 0.9689$ as data points were closer to each other and to the calibration line. Nevertheless, this again suggested that arsenic is distributed in a non-homogeneous manner in each phantom.

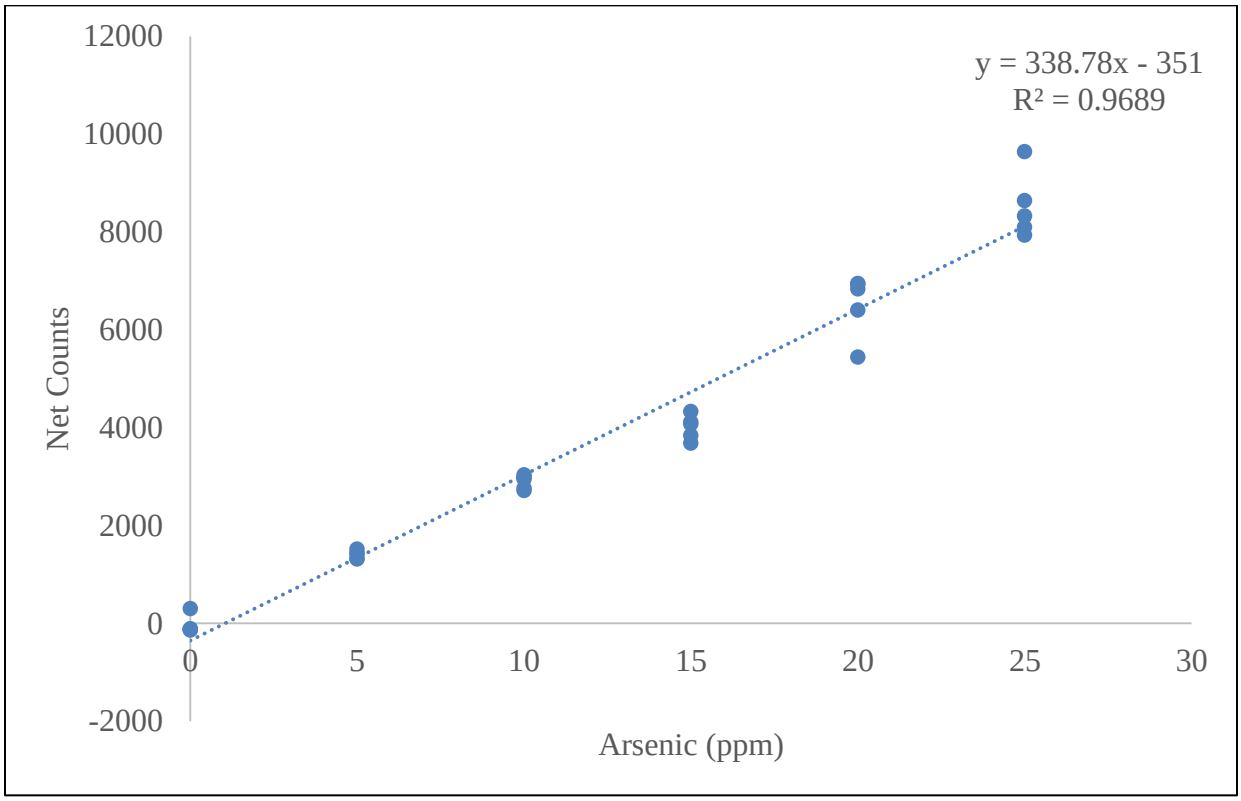

Figure 11 Calibration line using phantoms from Trial 3 for Set 2

In order to better compare the distribution of fluorescence data points and determine the homogeneity of the phantoms, both calibration lines were plotted together. This is shown in Figure 12. This was an important step towards understanding the errors in making a homogeneous arsenic-doped skin phantom set.

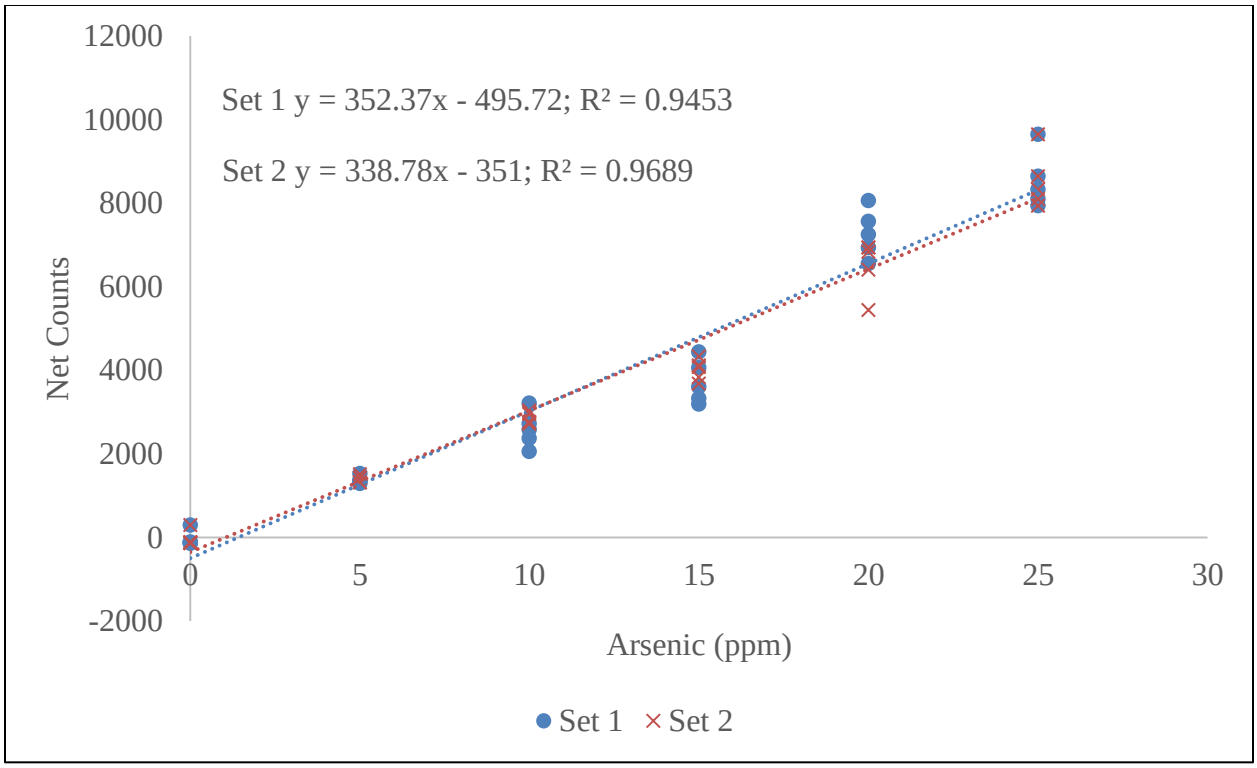

Figure 12 Comparison of both calibration lines from Trial 3

Phantoms from Trial 4 were produced based on closer attention to details and corrections to errors made in previous attempts. But, the phantom surface was not even and therefore the thickness was not uniform. Hence, three spots were selected based on opacity of phantoms to ensure consistency of arsenic distribution. This resulted in three fluorescence data points for each phantom. The fluorescence data and measured thickness was presented earlier in Table 3. Here, the calibration line plotted based on net counts is shown in Figure 13 below. As can be seen from the plot, the data points are very close to each other and sometimes overlap. The distance between the data points and calibration line is also minimal resulting in an improved R^2 value. The obtained $R^2 = 0.9961$ is significantly better compared to previous set of phantoms.

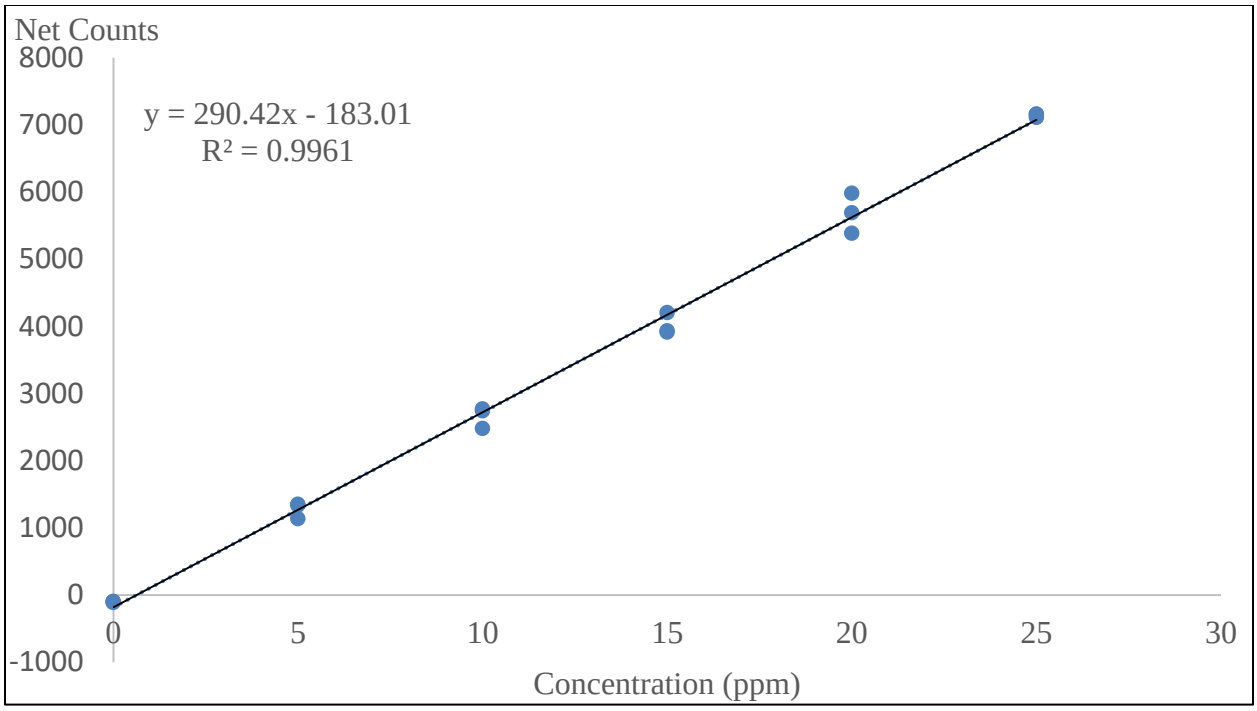

Figure 13 Calibration line for arsenic-doped skin phantoms from Trial 4

3.4 Calibration Lines for Skin Phantoms and Lucite Backing

Lucite was used as backing material to simulate the soft tissue layers beneath human skin. First, a 25ppm arsenic-doped skin phantom was measured for arsenic fluorescence data with a range of available lucite thickness. The purpose of this measurement was to determine the interaction of backscattered photons from varying thickness of underlying soft tissue and its effect on obtained arsenic fluorescence data. This will replicate *in vivo* measurement environment as different individuals will have varying soft tissue thickness. It is expected that the net counts from arsenic fluorescence will increase as more lucite thickness is added and saturate at a certain thickness. The measured data for this experimental setup is presented in Figure 14. In contrary to expected data distribution, the net counts obtained significantly drops after 10mm of lucite thickness.

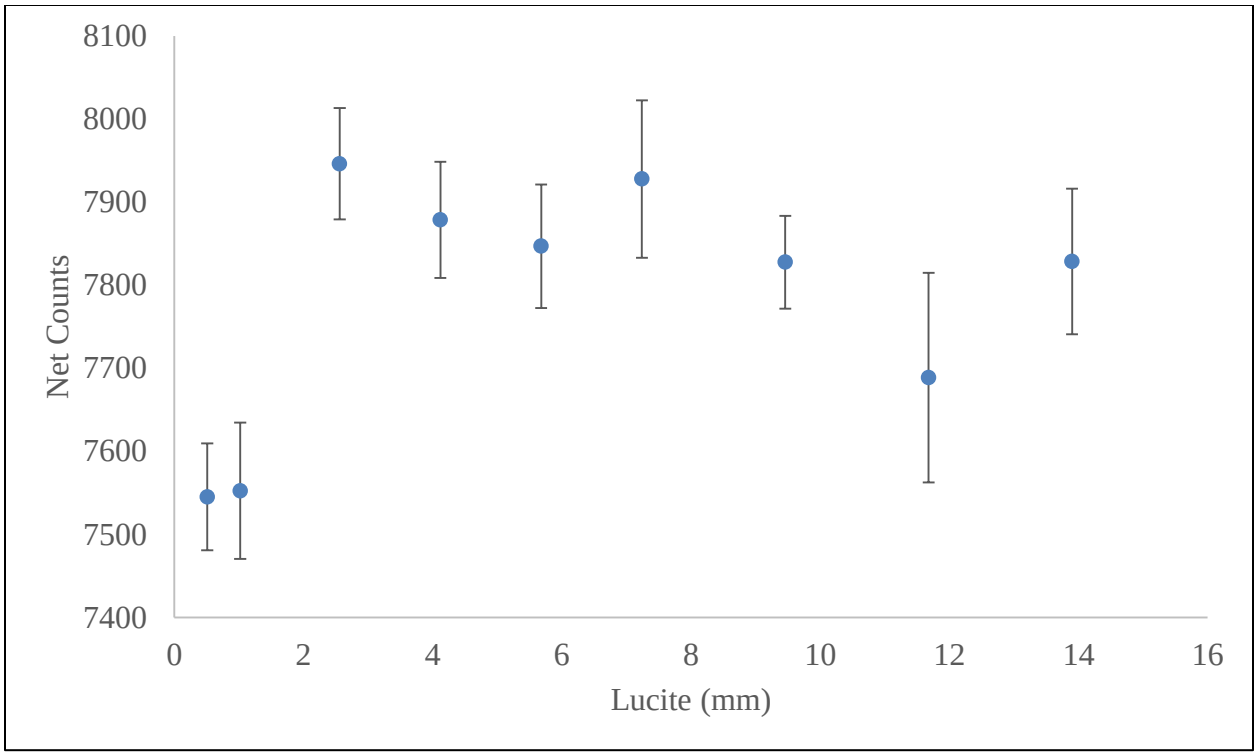

Figure 14 As Kα fluorescence net counts using 25 ppm arsenic-doped skin phantom for a range of lucite thickness, 0.51mm to 13.9mm

Next, only two lucite thickness of 4.44mm and 9.78mm were selected. Phantoms from Trial 4 were used to measure the net counts of arsenic fluorescence data. This was done to determine the feasibility of portable XRF device to detect As Kα signal intensity given thin and thick deposition of underlying soft tissues. The net counts were plotted against arsenic concentrations and calibration lines plotted in Figure 15 and 16 respectively for each lucite thickness. Error bars are included but are not visible due to their small range. The obtained R^2 for 4.44mm and 9.78mm lucite thickness are 0.9935 and 0.9949 respectively. This shows good correlation between measured net counts and corresponding arsenic value in each phantom given the presence of lucite backing material.

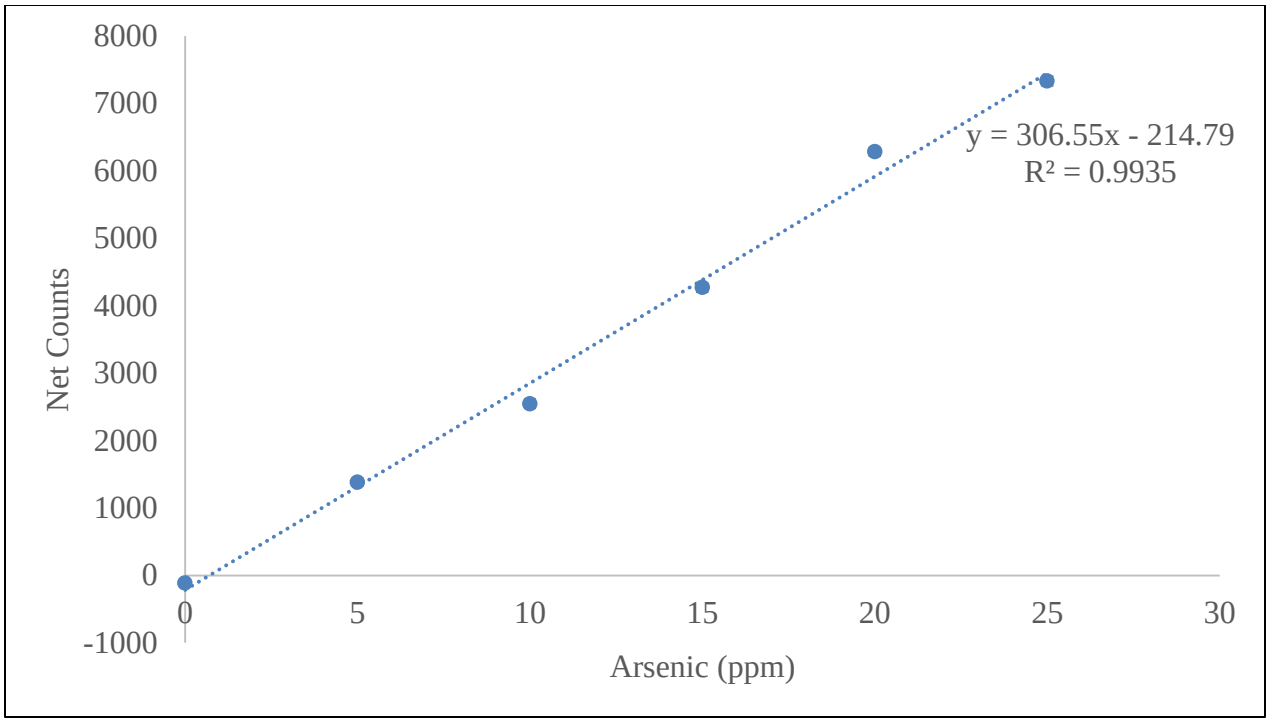

Figure 15 Calibration line based on phantoms from Trial 4 plotted against arsenic concentrations for 4.44mm of lucite

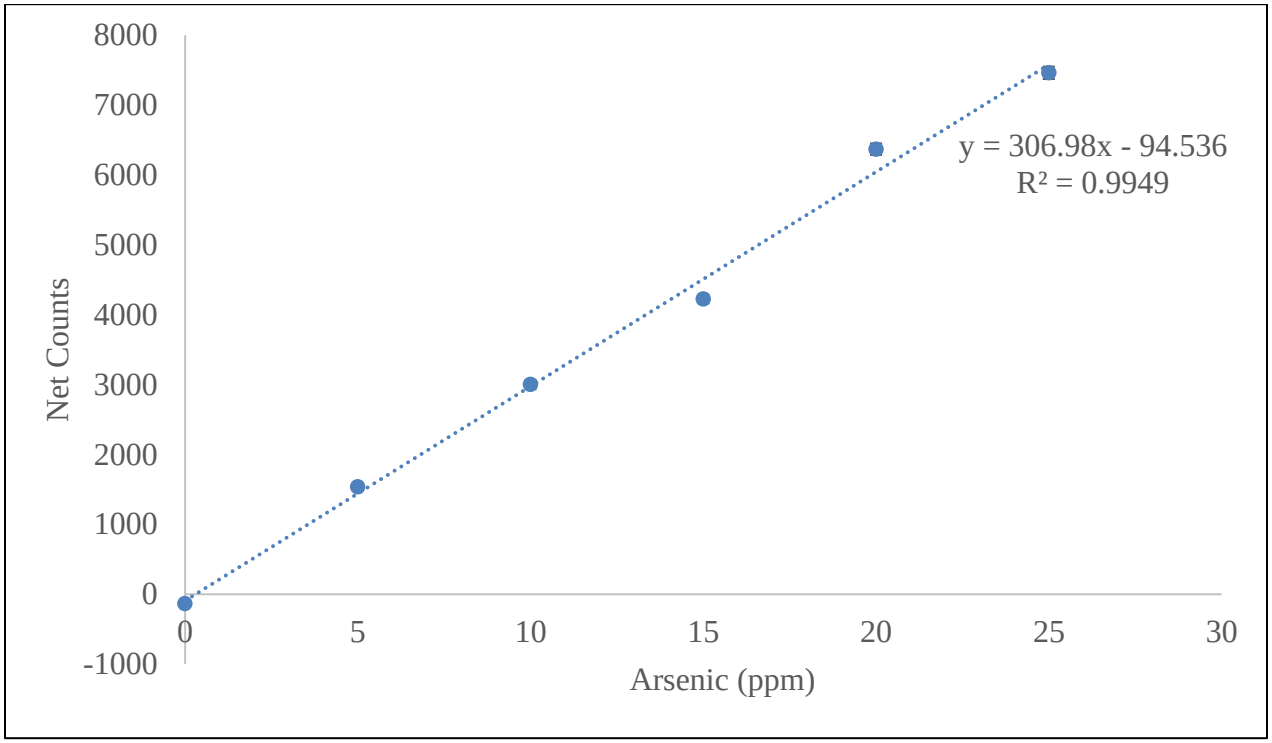

Figure 16 Calibration line based on phantoms from Trial 4 plotted against arsenic concentrations for 9.78mm of lucite

Both calibration lines for the different lucite thickness are combined and presented in a single plot below.

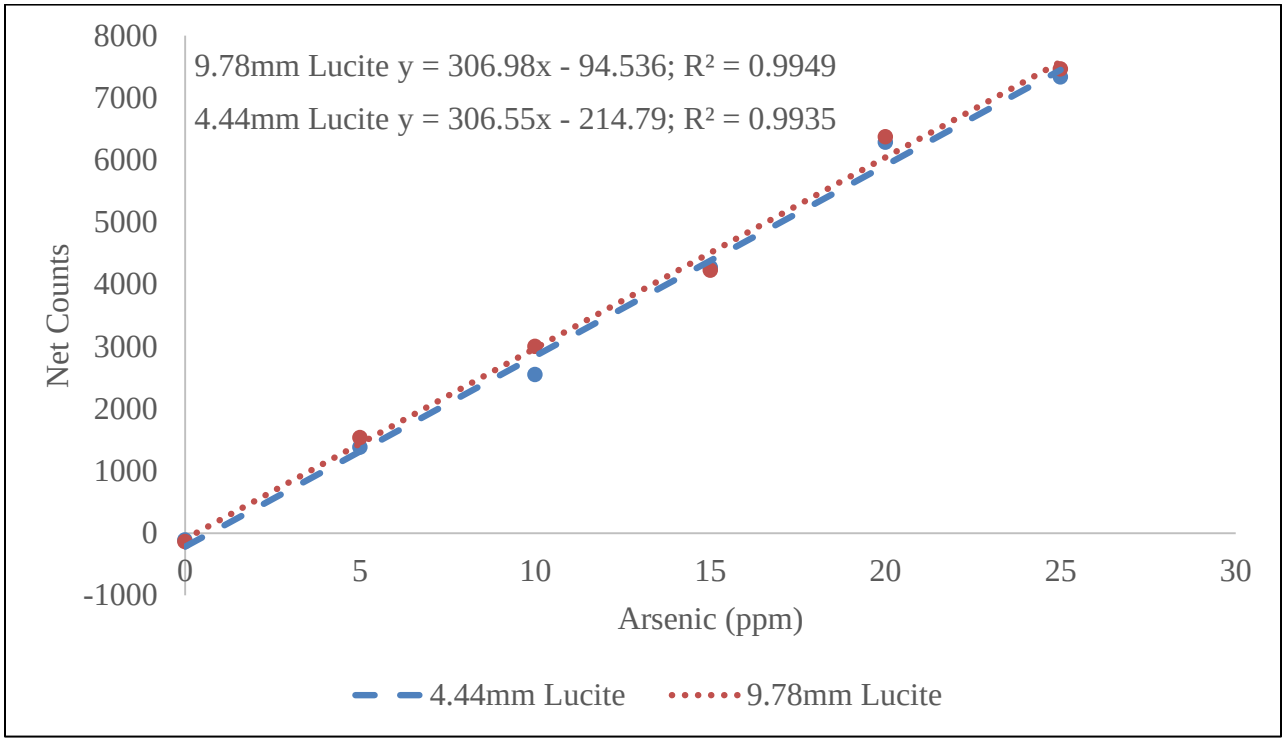

Figure 17 Comparison of calibration lines obtained for measurement of arsenic fluorescence data using phantoms from Trial 4 and lucite, 4.44mm and 9.78mm

The slope which gives the ratio of net counts to corresponding arsenic concentration shows significantly overlapping values for the two given lucite thickness. This shows that lucite thickness does not greatly affect arsenic signal detection for this portable XRF device.

3.5 Detection Limit of the System

The instrumental minimum detection limit (MDL) refers to the least quantity of element of interest, arsenic in this study, which can be detected by the portable device. The detection limit is based on background counts under peak of interest and the slope of calibration line. For this

study, the MDL was determined using Equation 2. This equation is commonly used in determination of MDL for XRF systems.

$$MDL = \frac{2\sqrt{BKG_{0ppm}}}{m} \qquad (2)$$

The BKG_{0ppm} in the equation refers to background counts under the As Kα peak obtained from all fluorescence data measured for 0ppm skin phantom which does not contain any amount of arsenic. In this equation, m refers to the slope of the calibration line, generated based on linear least-square method with y = mx+b.

In order to determine the background counts, the standard deviation (σ) for 25 ppm phantom was first identified. This was done using the fitted curve via Matlab where the c as mentioned in Equation 1 provides sigma value. Matlab also generates this value as width in its command window section. Based on this sigma value, the maximum and minimum energy range was identified by adding and subtracting 2σ from the As Kα peak central position respectively. Once this energy range was identified, all count rates within this energy range from 0 ppm which can be obtained from Excel spreadsheet was summed and multiplied with 180 seconds to get total counts. Now, this sum of counts was taken as background counts and squared in Equation 2.

Using the above mentioned steps, the MDL for bare phantoms from Trial 4 without any backing material was calculated. The width and arsenic peak position from the fitted curve for 25ppm were 0.07 and 10.57keV respectively. Based on this information, the energy range calculated is 10.42-10.71keV. Now, the measured fluorescence data from 0ppm based on the calculated energy range was summed to 3.19cps. This sum was multiplied with 180 seconds to get total

background counts which as was 574.14. Finally, the MDL was determined using Equation 2 which resulted in 0.17ppm (µg/g).

Next, the same steps were used to calculate the MDL values for the *in vivo* simulation environment based on phantoms with lucite backing material. The calculated values are summarized in the table below.

Table 4 Summary of values calculated to determine the instrumental minimum detection limit for phantoms with lucite backing

Lucite thickness (mm)	4.44	9.78
Standard deviation or width (σ)	0.08	0.07
2σ	0.15	0.15
As Kα peak position (keV)	10.57	10.56
Energy range (keV)	10.42 – 10.72	10.41 – 10.71
Total background counts	1005.33	1206.73
Slope	306.55	306.98
MDL (µg As/ g)	0.21	0.23

CHAPTER 4: DISCUSSION AND CONCLUSION

This current study investigated the feasibility of using the XL3t GOLDD+ portable XRF device to detect and quantify arsenic deposition in human skin. The system was validated using arsenic-doped skin phantoms to simulate human skin and lucite to mimic the underlying soft tissue layer. Also, minimum detection limit was determined in this study after performing system calibration and spectral analysis.

The nature of arsenic distribution in human skin besides its affinity towards keratin is unknown. It is not clear whether arsenic follows either homogeneous or inhomogeneous pattern in human skin. Furthermore, keratin is abundant in the superficial layers of the skin and hence constitutes only a thin portion of human skin. Since arsenic distribution in skin is not fully understood, the exact thickness for skin phantom is vague. The thickness of skin as measured via ultrasound in an earlier study using XRF for measuring arsenic in skin was in the range of 1.0-2.6mm (Studinski et al., 2005). Hence, arsenic-doped skin phantoms in the range of 1.5mm were attempted for this study.

The major challenge in this research was to produce a set of valid skin-equivalent phantoms. As mentioned earlier, it took four attempts to achieve an acceptable set of arsenic-doped skin phantoms using a mixture of fiberglass resin, salt solution, arsenic standard solution, and liquid hardener. Phantoms that were made in Trial 1 were not effectively produced. Some possible reasons for this are the less drops of liquid hardener added to the phantom mixture and extended time where the phantoms were left under the fume hood.

Although specific thicknesses, 1mm and 2mm, was attempted during the second trial, it was not feasible given the method used to achieve such values. The molds did not have exact thickness at either 1mm or 2mm. In order to achieve these thicknesses, the mass of phantom mixture was calculated and measured to fill the mold to the height of 1mm and 2mm. This method introduced errors associated with measurement of volumes of mold and mass of phantom mixture especially given the small values involved. Hence, this resulted in inconsistent phantom thickness. Not only that, the arsenic standard solution was not diluted in this trial. Volumes of arsenic solution in the microliter range were required to achieve the necessary arsenic concentrations in each phantom. However, the phantoms were removed from under the fume hood earlier than was allowed for in Trial 1 since low temperature was later determined as a factor that slows down the hardening process.

Phantoms produced during Trial 3 resulted in a widespread distribution of fluorescence data. This strongly suggested that the arsenic was not mixed well if not homogeneously. The time allowed for the phantom mixture to be mixed was short which could have led to uneven deposition of arsenic. Besides that, the phantom opacity changed throughout its hardening duration under the fume hood. This pattern was observed in phantoms produced in Trial 4. The possible explanation for this phenomenon is evaporation. The phantoms were left under the fume hood where evaporation could have affected the solution before it settled uniformly. Thus, three spots were selected for each phantom where the opacity was uniform in order to ensure consistency. The fluorescence data measured for the spots resulted in improved conformity with the expected distribution. Hence, the phantoms from Trial 4 were used to perform other experimental measurements.

In this study, lucite was used as a backing material to simulate soft tissue. As mentioned earlier, the net counts obtained using 25ppm arsenic-doped skin phantom for varying lucite thickness was expected to increase and then saturate. This is because the added backing layer will generate backscattered photons that redirect into the skin phantom and produce more arsenic fluorescence signal intensity. However, the experimental data does not conform to this pattern. Instead, the net counts begin dropping after using approximately 10mm of lucite. The reason for this distribution is unknown. A possible explanation for such reduction in net counts is the presence of air gap between the lucite layers and phantom surface. This is because the lucite slabs have flat and even surface. Furthermore, the geometry effect is less because the phantom was held in the same position using a tape while slabs of lucite were added for multiple measurements.

The minimum detection limit (MDL) achieved in this research is compared against similar studies in recent times. In this study, the XL3t GOLDD+ portable XRF device was set to 50kV, 40μA, and combined with silver filter that resulted in a MDL value of 0.17ppm using bare phantoms. The MDL increased to 0.21ppm and 0.23ppm upon adding 4.44mm and 9.78mm lucite as backing material for the phantoms. These values are lower than that achieved by recent studies using the Olympus Innov-X Delta models. One study achieved 0.462±0.002ppm (Desouza et al., 2017) while another study obtained 0.59±0.03ppm (Shehab, 2016). Since the measurement times are different for these studies, the MDL values must be normalized to 3 minutes to be compared with the MDL obtained in this current research. If the aforementioned studies were to be conducted for 180 seconds as in this current research, the MDL values will improve by $\sqrt{1.5}$ and $\sqrt{3}$ to yield 0.38ppm and 0.34ppm respectively. Based on available skin-

scales data among population exposed to arsenic, the arsenic concentration has been reported with a geometric mean of 0.90ppm (Samanta, Sharma, Roychowdhury, & Chakraborti, 2004). Hence, the portable device used in this current research is able to detect and quantify arsenic concentration among population in arsenic contaminated areas. There are some reasons for which the MDLs achieved in this research are lower in comparison to literature. Firstly, the tube settings of voltage and current are higher which results in greater photon production. High tube voltage increases energy of photons while high tube current releases more electrons from the target material. This combined effect will produce higher intensity of photons. Next, this research performed 180 seconds of measurement time in contrary to 120 seconds (Desouza et al., 2017) and 60 seconds (Shehab, 2016). Longer measurement time allows for more detection of arsenic fluorescence resulting in greater peak intensity.

However, there are more improvements that can be made in future works. A better method that can be used in future works is to make a thick phantom and slice it to the desired thickness. This will produce phantoms with uniform thickness across the surface. It is safe to assume that arsenic distribution in human skin is homogenous for the purpose of making phantoms until more information is available. Besides that, the device can be further optimized by comparing the experimental values to simulation generated using Monte Carlo methods. This will provide more details on the ideal tube settings for arsenic detection. Since the long-term goal of this project is to measure arsenic exposure based on skin under heels as measurement site, an actual trial can be performed to determine the response of the device *in vivo*. This will also provide information that can be compared against skin phantoms to determine if the calibration phantoms match *in vivo*

environment. Finally, dosimetry test must be conducted based on the tube settings to determine if the device is suitable for clinical purposes.

REFERENCES

Agusa, T., Trang, P. T. K., Lan, V. M., Anh, D. H., Tanabe, S., Viet, P. H., et al. (2014). Human exposure to arsenic from drinking water in Vietnam. *Science of the Total Environment, 488-489*(1), 562-569.

Allan, H. S., Ayse, E., Yan, Y., & Craig, M. S. (2009). Increased lung cancer risks are similar whether arsenic is ingested or inhaled. *Journal of Exposure Science and Environmental Epidemiology, 19*(4), 343.

Arsenic Public Health Statement. (2007). *Public Health Statements* Retrieved 03/05, 2018

Basu, A., & Schreiber, M. E. (2013). Arsenic release from arsenopyrite weathering: Insights from sequential extraction and microscopic studies. *Journal of Hazardous Materials, 262*, 896-904.

Desouza, E. D., Gherase, M. R., Fleming, D. E. B., Chettle, D. R., O'meara, J. M., & McNeill, F. E. (2017). Performance comparison of two Olympus InnovX handheld x-ray analyzers for feasibility of measuring arsenic in skin in vivo – Alpha and Delta models. *Applied Radiation and Isotopes, 123*(C), 82-93.

Ferreccio, C., González, C., Milosavjlevic, V., Marshall, G., Sancha, A. M., & Smith, A. H. (2000). Lung Cancer and Arsenic Concentrations in Drinking Water in Chile. *Epidemiology, 11*(6), 673-679.

Groskopf, C., Bennett, S. R., Gherase, M. R., & Fleming, D. E. B. (2017). Detection of lead in bone phantoms and arsenic in soft tissue phantoms using synchrotron radiation and a portable x-ray fluorescence system. *Physiological Measurement, 38*(2), 374-386.

Guo, H.-R., Yu, H.-S., Hu, H., & Monson, R. (2001). Arsenic in drinking water and skin cancers: cell-type specificity (Taiwan, R.O.C.). *Cancer Causes & Control, 12*(10), 909-916.

Hsueh, Y. M., Chiou, H. Y., Huang, Y. L., Wu, W. L., Huang, C. C., Yang, M. H., et al. (1997). Serum β-carotene level, arsenic methylation capability, and incidence of skin cancer. *Cancer Epidemiology Biomarkers and Prevention, 6*(8), 589-596.

Karagas, M., Tosteson, T., Morris, J., Demidenko, E., Mott, L., Heaney, J., et al. (2004). Incidence of Transitional Cell Carcinoma of the Bladder and Arsenic Exposure in New Hampshire. *Cancer Causes & Control, 15*(5), 465-472.

Kim, E. J., Yoo, J.-C., & Baek, K. (2014). Arsenic speciation and bioaccessibility in arsenic-contaminated soils: Sequential extraction and mineralogical investigation. *Environmental Pollution, 186*(C), 29-35.

Komorowicz, I., & BaraAkiewicz, D. (2016). Determination of total arsenic and arsenic species in drinking water, surface water, wastewater, and snow from Wielkopolska, Kujawy-Pomerania, and Lower Silesia provinces, Poland.(Report). *188*(9), 1.

Lai, M.-S., Hsueh, Y.-M., Chen, C.-J., Shyu, M.-P., Chen, S.-Y., Kuo, T.-L., et al. (1994). Ingested Inorganic Arsenic and Prevalence of Diabetes Mellitus. *American Journal of Epidemiology, 139*(5), 484.

Lazarević, K., Nikolić, D., Stosić, L., Milutinović, S., Videnović, J., & Bogdanović, D. (2012). Determination of lead and arsenic in tobacco and cigarettes: an important issue of public health. *Cent Eur J Public Health, 20*(1), 62-66.

Loffredo, C. A., Aposhian, H. V., Cebrian, M. E., Yamauchi, H., & Silbergeld, E. K. (2003). Variability in human metabolism of arsenic. *Environmental Research, 92*(2), 85-91.

McIver, D. J., VanLeeuwen, J. A., Knafla, A. L., Campbell, J. A., Alexander, K. M., Gherase, M. R., et al. (2015). Evaluation of a novel portable x-ray fluorescence screening tool for detection of arsenic exposure. *Physiological Measurement, 36*(12), 2443-2459.

Nie, L. H., Sanchez, S., Newton, K., Grodzins, L., Cleveland, R. O., & Weisskopf, M. G. (2011). in vivo quantification of lead in bone with a portable x-ray fluorescence systemmethodology and feasibility. *Physics in Medicine and Biology, 56*(3), N39-N51.

O'Shea, B., Stransky, M., Leitheiser, S., Brock, P., Marvinney, R. G., & Zheng, Y. (2015). Heterogeneous arsenic enrichment in meta-sedimentary rocks in central Maine, United States. *The Science of the Total Environment, 505*, 1308.

Popovic, M., Chettle, D. R., McNeill, F. E., & Pejović-Milić, A. (2006). Improvement in the detection limit of anin vivo XRF cadmium detection system. *An International Journal Dealing with All Aspects and Applications of Nuclear Chemistry, 269*(2), 421-424.

Rahman, M., Tondel, M., Ahmad, S. A., & Axelson, O. (1998). Diabetes mellitus associated with arsenic exposure in Bangladesh. *American journal of epidemiology, 148*(2), 198.

Samanta, G., Sharma, R., Roychowdhury, T., & Chakraborti, D. (2004). Arsenic and other elements in hair, nails, and skin-scales of arsenic victims in West Bengal, India. *The Science of the total environment, 326*(1-3), 33.

Shehab, H. (2016). Feasibility of measuring arsenic and selenium in human skin using in vivo x-ray fluorescence (XRF)--a comparison of methods. *Physiological Measurement, 37*(1), 145.

Specht, A. J., Mostafaei, F., Lin, Y., Xu, J., & Nie, L. H. (2017). Measurements of Strontium Levels in Human Bone In Vivo Using Portable X-ray Fluorescence (XRF). *Applied Spectroscopy, 71*(8), 1962-1968.

Specht, A. J., Weisskopf, M., & Nie, L. H. (2014). Portable XRF Technology to Quantify Pb in Bone. *Journal of Biomarkers, 2014*.

Studinski, R. C. N., McNeill, F. E., Chettle, D. R., & O'Meara, J. M. (2005). Estimation of a method detection limit for an in vivo xrf arsenic detection system. *Physics in Medicine and Biology, 50*(3), 521-530.

Studinski, R. C. N., McNeill, F. E., O'Meara, J. M., & Chettle, D. R. (2006). Amethod detection limit for potential in vivo arsenic measurements with a 50 w x-ray tube. *Physics in Medicine and Biology, 51*(21), N381-N387.

Styblo, M., Del Razo, L. M., Lecluyse, E. L., Hamilton, G. A., Wang, C., Cullen, W. R., et al. (1999). Metabolism of arsenic in primary cultures of human and rat hepatocytes. *Chemical research in toxicology, 12*(7), 560.

Su, C.-C., Lu, J.-L., Tsai, K.-Y., & Lian, I.-B. (2011). Reduction in arsenic intake from water has different impacts on lung cancer and bladder cancer in an arseniasis endemic area in Taiwan. *An International Journal of Studies of Cancer in Human Populations, 22*(1), 101-108.

Tseng, C.-H. (2002). An Overview on Peripheral Vascular Disease in Blackfoot Disease-Hyperendemic Villages in Taiwan. *Angiology, 53*(5), 529-537.

Tseng, C.-H. (2005). Blackfoot Disease and Arsenic: A Never-Ending Story. *Journal of Environmental Science and Health, Part C, 23*(1), 55-74.

Tseng, C.-H., Huang, Y.-K., Huang, Y.-L., Chung, C.-J., Yang, M.-H., Chen, C.-J., et al. (2005). Arsenic exposure, urinary arsenic speciation, and peripheral vascular disease in blackfoot disease-hyperendemic villages in Taiwan. *Toxicology and Applied Pharmacology, 206*(3), 299.

Vladimir, B., & Florence Yan Li, F. (2017). The history of arsenical pesticides and health risks related to the use of Agent Blue. *Annals of Agricultural and Environmental Medicine, 24*(2), 312-316.

Xue, J., Zartarian, V., Wang, S.-W., Liu, S. V., & Georgopoulos, P. (2010). Probabilistic modeling of dietary arsenic exposure and dose and evaluation with 2003-2004 NHANES data.(Research)(Report). *Environmental Health Perspectives, 118*(3), 345.

Zhang, X., Specht, A. J., Weisskopf, M. G., Weuve, J., & Nie, L. H. (2018). Quantification of manganese and mercury in toenail in vivo using portable X-ray fluorescence (XRF). *Biomarkers, 23*(2), 154-160.